The Impact of High-Resolution Sea Surface Temperatures on the Simulated Nocturnal Florida Marine Boundary Layer

KATHERINE M. LACASSE

University of Alabama in Huntsville, Huntsville, Alabama

MICHAEL E. SPLITT AND STEVEN M. LAZARUS

Florida Institute of Technology, Melbourne, Florida

WILLIAM M. LAPENTA

NASA Marshall Space Flight Center, Huntsville, Alabama

(Manuscript received 6 February 2007, in final form 24 July 2007)

ABSTRACT

High- and low-resolution sea surface temperature (SST) analysis products are used to initialize the Weather Research and Forecasting (WRF) Model for May 2004 for short-term forecasts over Florida and surrounding waters. Initial and boundary conditions for the simulations were provided by a combination of observations, large-scale model output, and analysis products. The impact of using a 1-km Moderate Resolution Imaging Spectroradiometer (MODIS) SST composite on subsequent evolution of the marine atmospheric boundary layer (MABL) is assessed through simulation comparisons and limited validation. Model results are presented for individual simulations, as well as for aggregates of easterly- and westerly-dominated low-level flows. The simulation comparisons show that the use of MODIS SST composites results in enhanced convergence zones, earlier and more intense horizontal convective rolls, and an increase in precipitation as well as a change in precipitation location. Validation of 10-m winds with buoys shows a slight improvement in wind speed. The most significant results of this study are that 1) vertical wind stress divergence and pressure gradient accelerations across the Florida Current region vary in importance as a function of flow direction and stability and 2) the warmer Florida Current in the MODIS product transports heat vertically and downwind of this heat source, modifying the thermal structure and the MABL wind field primarily through pressure gradient adjustments.

1. Introduction

Predicting mesoscale phenomena affecting the spatial and temporal distribution of temperature, wind, and precipitation is a common forecast challenge along the Florida peninsula (e.g., Bauman and Businger 1996). Large gradients in sea surface temperature (SST) east of central Florida associated with the Florida Current (FC) during the late spring and summer have a direct impact on the development of offshore secondary solenoids (Sublette and Young 1996), cumulus cloud lines (Li et al. 2004), and stratocumulus cloud fields. Figure 1 shows cloud features on 17 May 2004 that typify some of the complex SST-influenced features of the summer season. Features of note include a low-level cumulus field over the FC, north of the Bahamas, horizontal convective rolls associated with and downwind of the Bahamas, and convection over the Florida–Hatteras shelf (FHS) along the western edge of the FC. Figure 1 also depicts a lack of cumulus over the cooler FHS waters and a relatively clear region west of the Florida peninsula as easterly low-level flow moves from the warmer peninsula to the cooler SSTs.

Numerous studies using satellite-derived and conventional observations have shown a positive correlation between SST fields and near-surface wind stress at scales of 1000 km or less (e.g., Chelton et al. 2001; O'Neill et al. 2003; Tokinaga et al. 2005). Modeling

Corresponding author address: Katherine M. LaCasse, University of Alabama in Huntsville, 320 Sparkman Dr., Huntsville, AL 35805.
E-mail: kate.lacasse@nasa.gov

DOI: 10.1175/2007MWR2167.1

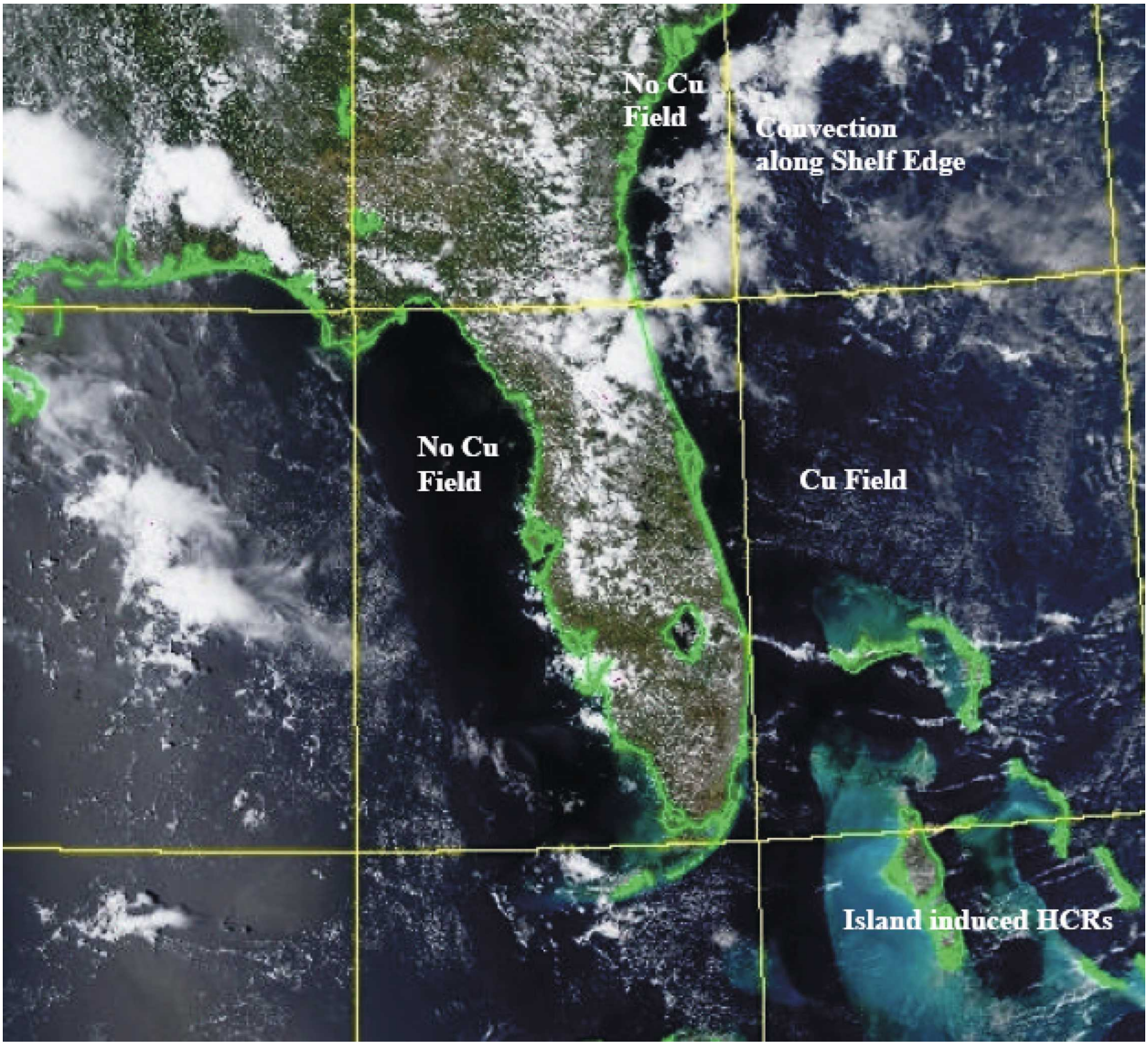

FIG. 1. MODIS visible composite valid at 1855 UTC 17 May 2004. Cloud features of note include a low-level cumulus field over the Florida Current, horizontal convective rolls associated with and downwind of the Bahamas, convection over the Florida–Hatteras shelf along the western edge of the Florida Current, and a lack of cumulus over the cooler Florida–Hatteras shelf waters and west of the Florida peninsula.

studies have also simulated this relationship. Small et al. (2003) explored the importance of three processes involved in the response of the marine atmospheric boundary layer (MABL) to tropical instability waves using a regional climate model. For that case, vertical mixing was important to latent and sensible heat fluxes and horizontal mixing had a small effect by advecting the SST impact downstream. The horizontal perturbation pressure gradient was shown to be significant, because it drove the near-surface wind speed changes across the SST gradients. In a study by Song et al. (2004), the fifth-generation Pennsylvania State University–National Center for Atmospheric Research Mesoscale Model (MM5) was used to study the impact of a SST front on the MABL at high resolution (3-km grid resolution). Two separate cases were evaluated, and the simulated MABL response to the imposed SST fields compared well to the observations collected via aircraft. This result lends confidence to the claim that the use of high-resolution SSTs in a mesoscale model can produce a realistic simulation of the MABL. Chelton (2005) investigated the impact of SST spatial resolution using the European Centre for Medium-Range Weather Forecast (ECMWF) system. Forecasts were

conducted and compared using the 1° Reynolds SST field and the 0.5° real-time global (RTG) SST analyses. Use of higher-resolution SST data resulted in forecasts that compared more favorably with near-surface wind stress as derived from the National Aeronautics and Space Administration (NASA) Quick Scatterometer (QuikSCAT) instrument on board the Tropical Rainfall Measuring Mission (TRMM) Microwave Imager (TMI). Initialization of a mesoscale model with calm wind and flat horizontal pressure gradients showed a direct correlation between the strength of the SST gradient and simulated thermal and moisture gradients within the MABL associated with an atmospheric front in the vicinity of the Gulf Stream (Warner et al. 1990). Despite the various boundary layer formulations used, each of these studies indicates sensitivity to the underlying specification of the SST.

As the horizontal resolution of operational numerical weather prediction models continues to increase, it has become increasingly important to properly specify the spatial heterogeneity associated with land surface forcing (i.e., soil moisture, vegetation characteristics, etc.). While the diurnal signal of SST is typically much less than that over land, in calm conditions it can be significant (Minnett 2003). Moreover, resolving SST features, especially mesoscale gradients in the near-shore environment, is inarguably an essential component with respect to the improvement of coastal zone forecasts of boundary layer clouds and precipitation, accurate specification of surface fluxes, etc. Current operational forecast Models [e.g., the North American Mesoscale (NAM) model and the ECMWF model] are initialized with a 0.5° SST analysis produced daily at the National Centers for Environmental Prediction (NCEP; Thiébaux et al. 2003). The purpose of this study is to examine the impact of using high-resolution (1 km) SST fields derived from the NASA Earth Observing System Moderate Resolution Imaging Spectroradiometer (MODIS) on the overlying MABL thermodynamic and kinematic structures as simulated by the Weather Research and Forecasting (WRF; Skamarock et al. 2005) modeling system run at 2-km resolution over the Florida peninsula.

The paper is structured as follows. Sea surface temperature products are described in section 2. Section 3 contains a description of the WRF configuration and experiment design. Results are presented in section 4, followed by the summary, conclusions, and suggestions for future work in section 5.

2. Sea surface temperature products

The purpose of this study is to examine and understand how the spatial resolution of SST fields used within a state-of-the-art numerical weather prediction system affects simulations of MABL evolution and structure. Therefore, two SST products are employed. The first is the operational NCEP RTG product that is used in the NCEP operational NAM and Global Forecast System modeling suite. The RTG is the default SST field used by the majority of the WRF user community. The second is a prototype SST product derived from MODIS that is not yet available to the WRF community.

a. Real-time global sea surface temperature analysis

The RTG SST analysis is produced daily by the NCEP Marine Modeling and Analysis Branch. The analysis is created using a two-dimensional variational data assimilation scheme, with the previous analysis, adjusted for climatology, providing the background field (Thiébaux et al. 2003). Observations from the past 24 h, as well as previously unused in situ observations up to 36 h old, are averaged within each grid box for each observation type. The observations include ship and buoy data as well as satellite-derived SST from the National Oceanic and Atmospheric Administration Advanced Very High Resolution Radiometer. A spatially varying Gaussian error decorrelation length scale is defined to be inversely proportional to the climatological SST gradients (Thiébaux et al. 2003). This ensures that the SST observations are given a smaller (larger) radius of influence in regions of strong (weak) SST gradients. Global analyses are created operationally once daily at both 0.5° and 0.083° spatial resolution. Only the 0.5° product was available during the case study period of May 2004 and is used for the WRF RTG simulations herein. The RMS errors for this product, in comparison with those of buoys, range between 0.4°–0.6°C for 30°S–30°N and 0.6°–1.2°C for 30°–90°N (Thiébaux et al. 2003). The 0.5° grid also provides the SSTs for numerous operational models, including the NAM, the rapid update cycle (RUC), and the ECMWF models.

b. MODIS sea surface temperature composite

The MODIS instrument, on both the NASA *Aqua* and *Terra* polar-orbiting satellites, uses clear-sky infrared channels to retrieve SST. In particular, brightness temperature from both the 11- and 12-μm channels, as well as a climatological estimate of SST, contributes to the MODIS SST value. These SST products have been compared with buoys and have errors of 0.5°C (Minnett et al. 2007).

The 1-km MODIS SST composite used in this work is a prototype dataset currently produced at the NASA

Short-Term Prediction Research and Transition (SPoRT) Center. It is produced by combining multiple passes of the 1-km Earth Observing System MODIS SST data in order to reduce spatial gaps caused by pass location and/or cloud contamination. The compositing approach is based on the assumption that the day-to-day variation of SST is relatively small. The validity of this assumption may vary spatially and seasonally as oceanic and atmospheric forcing creates higher-frequency changes in SST values (e.g., cooling in the wake of a hurricane). Data from both MODIS platforms are combined to create separate day/night composites using the five most recent clear-sky SST values for each pixel. Daytime (nighttime) *Aqua* and *Terra* passes through the composite region occur at approximately 1330 and 1030 (approximately 0130 and 2230) LT, respectively. Four distinct composites are created daily by combining data that correspond to the same time of day in order to capture as much of the diurnal signal as possible. The composite method used for this study averages the warmest three of the five pixels in order to mitigate the impact of cloud contamination. For the month of May 2004, the warmest pixels are also the most recent.

The MODIS SST composites used in this study have been verified against buoys and appear to represent the SST field well with RMS errors less than 0.7°C (Haines et al. 2007). A comparison of the MODIS composite with a clear MODIS pass reveals that the composite retains the strength of the SST gradients (not shown). Alternative compositing methodologies are currently under development in an attempt to decrease product latency, while capturing short-term changes in the SSTs (S. L. Haines 2006, personal communication).

c. *A comparison of RTG and MODIS SST products*

A representative day (13 May 2004) from the study period is chosen to highlight the differences between the MODIS SST composites and RTG SST analyses. Figure 2 shows both fields after being mapped onto the 2-km WRF grid used for this study. The large-scale structures observed in the SST fields are similar, as expected, with values varying by only 1°C. However, the MODIS SST composite clearly has more finescale detail than the RTG SST analysis, both offshore and along the immediate coast. The Florida Current and Gulf Stream are discontinuous off the northern Florida coast and are poorly resolved in the RTG. In addition, the RTG SST analysis underestimates the southern extent of the near-shore cool wedge off the east coast of Florida, resulting in temperatures 0.5°–2°C warmer than the MODIS SST composite.

Differences between the analyses described above persist throughout May 2004 and have a relatively significant impact on the magnitude and location of the SST gradient along the western edge of the Florida Current. Figure 3 shows a plot of the two SST analyses across the western boundary of the Florida Current, as well as the heat content within the Florida Current. The MODIS SST composite exhibits a gradient of approximately 2°C in a 40-km distance, while the SST in the RTG analysis is virtually flat and exhibits no gradient at all. The absence of such mesoscale SST features will be shown to have an impact on the simulation of the MABL and associated sensible weather elements in coastal regions.

3. Model description and experiment design

A coupled atmospheric data assimilation and forecast system was employed to examine the impact of high-resolution SST fields on simulated MABL structures using real data cases. A description of the data assimilation, model configuration, and a detailed description of the experiment design follows.

a. *ARPS Data Analysis System*

The Advanced Regional Prediction System (ARPS; Xue et al. 2000) consists of several components, including a data assimilation system [ARPS Data Analysis System (ADAS)]. The ADAS is used to generate initial conditions for the WRF model used in this study. It is an iterative successive correction scheme, commonly referred to as the Bratseth method, which converges to optimal interpolation (Bratseth 1986). This scheme is convenient because it is computationally less demanding than other data assimilation methods (such as variational techniques). The number of iterations, type of data, and order of assimilation are user controlled, which preferentially allows the large-scale observations to adjust the background field, followed by the smaller-scale data. The error variances assigned to the observations and the background field, as well as the distances between observations and grid points, determine how much influence the observations will have on the analysis. Horizontal and vertical scaling distances are also specified for each iteration, and errors are specified for each type of observation. The assimilation method is further described in Brewster (1996) and Lazarus et al. (2002).

Observations assimilated in this study include the Aviation Routine Weather Reports (METARs), buoys, Aircraft Communication Addressing and Reporting System (ACARS), rawinsondes, wind profilers, and

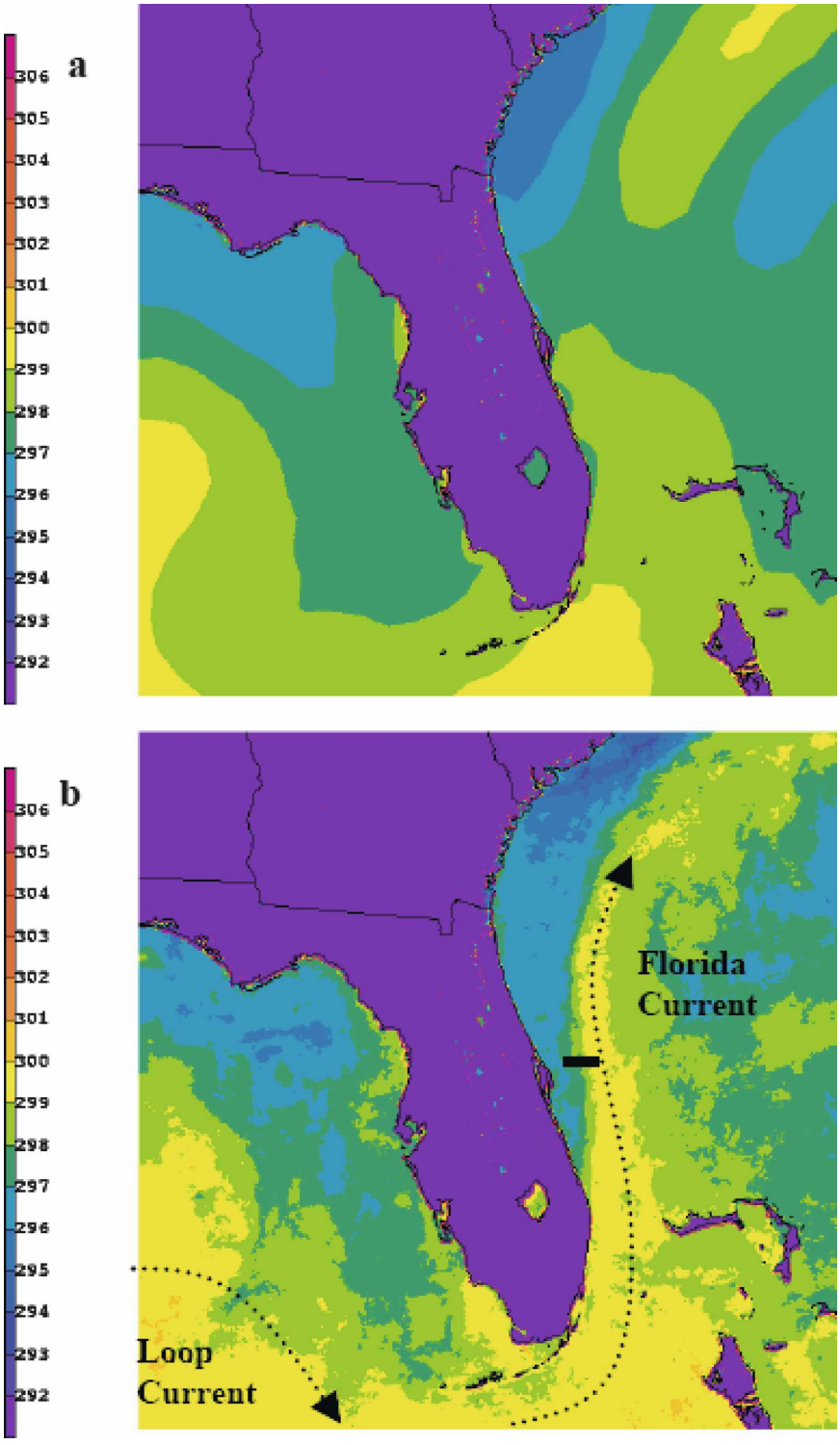

FIG. 2. SSTs (K) mapped to the WRF domain (2-km resolution) valid 13 May 2004 for (a) RTG SST analysis and (b) daytime *Aqua* MODIS SST composite. The solid black line east of Cape Canaveral in (b) indicates the cross section depicted in Fig. 3. Dotted lines represent the significant ocean currents within the domain.

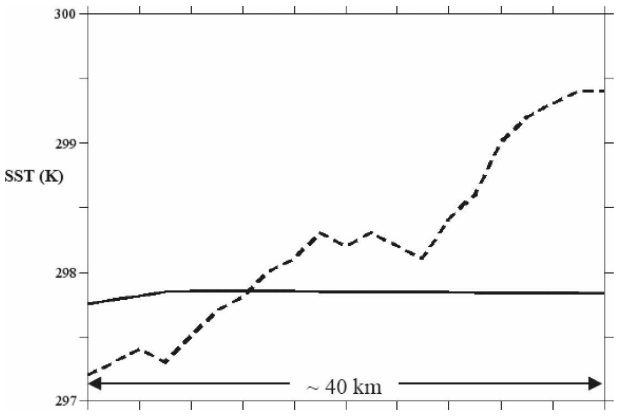

FIG. 3. Value of RTG SST (solid) and MODIS SST (dashed) as described in Fig. 2. Line is taken at 29.01°N latitude and 80.49°–80.10°W longitude, as drawn on Fig. 2b.

Florida Weather Surveillance Radar-1988 Doppler (WSR-88D) level II radar radial winds. Estimates of observation errors for these commonly used data types are provided with the ARPS code, and for this study, the default values are used. The observations are analyzed on the three-dimensional ADAS grid for the u and v component of the wind, pressure, potential temperature, and specific humidity. Quality control measures include a buddy check with nearby observations and a comparison with the background field. Surface data are also checked against observations from a prior time, in this case the previous hour. The WSR-88D level II radar data are remapped for the ARPS grid by averaging the data within each 3D grid box and reformatting the data for the ADAS (Brewster 1996).

The proper specification of land surface conditions for this study is an important component of the experiment design because the diurnal variation of the planetary boundary layer (PBL) over land is known to be a strong forcing factor in the development and evolution of mesoscale atmospheric phenomena in the Florida coastal regions. The best possible representation of soil moisture conditions for the study period was obtained using antecedent precipitation and near-surface meteorological data over a 4-month period in an offline mode to force the soil model. To obtain the best possible definition of the coastline, the 3-s U.S. Geological Survey data were used.

b. The WRF prediction system

The WRF prediction system consists of two dynamical cores—the Advanced Research WRF (version 2.1.0 is used herein) and the Nonhydrostatic Mesoscale Model. The WRF model is modular, allowing users to easily select different combinations of physics schemes, and it is optimized for parallel computing environments. The physics options used in this study include the Noah land surface model, the Yonsei University (YSU) PBL scheme, WRF single-moment six-class (WSM-6) microphysics, Dudhia shortwave radiation, and Rapid Radiative Transfer Model (RRTM) longwave radiation. To properly gauge the impact of the SSTs, the components involving surface–atmosphere interaction are of particular importance. The four-layer soil temperature and moisture model, Noah (Chen and Dudhia 2001), provides heat and moisture fluxes for the YSU PBL scheme (Hong et al. 2006). The YSU PBL scheme uses nonlocal K mixing and treats entrainment at the top of the PBL explicitly. The YSU PBL scheme was chosen after comparisons against the Mellor–Yamada–Janjić (Mellor and Yamada 1982; Janjić 1994) turbulent kinetic energy (TKE) PBL scheme revealed relatively small differences in the control forecasts and comparable impact due to the MODIS SSTs (not shown). However, in some instances, the scheme-to-scheme (PBL) variability is on the order of that of the impact of the SSTs on the simulations. This choice is consistent with recently published work of Song et al. (2006), which indicates that MM5 simulations using the MRF PBL scheme (i.e., the YSU predecessor) yielded the best results of the five boundary layer models when compared directly against observations.

c. Experiment design

WRF simulations were conducted over a region that includes Florida, the eastern Gulf of Mexico, and the Atlantic coastal waters of east Florida (Fig. 2). The domain consists of 500 × 500 horizontal grid points at 2-km resolution with 51 vertical levels. The lowest sigma levels were spaced every 0.01 between 1.00 and 0.90, which is a sufficient resolution for the calculation of surface fluxes (Hong et al. 2006). A series of 24-h simulations conducted each day during May 2004 were initialized at 0000 UTC. The National Climate Data Center (NCDC) ranked May 2004 as the fourth driest May on record for the state of Florida for the period of 1895–2004 (NCDC 2004). May 2004 was selected for this study because it represented a relatively clear period when few synoptic-scale frontal systems propagated south of 30°N, allowing the marine boundary layer to be strongly modulated by the underlying SST. Although a period with clouds and precipitation would also be of interest, it was our desire to mitigate complications associated with convection. Because of the quiescent period chosen, the impact of the MODIS SSTs will be primarily confined to the MABL. Addi-

tional benefits of choosing a dry period include the following: 1) fewer cloud-contaminated pixels, resulting in reduced composite latency, and 2) weak synoptic flow, which enables the configuration of a solitary, computationally efficient model grid without the introduction of spurious boundary condition problems resulting from large-scale forcing.

Two sets of numerical experiments were performed. One model configuration (experiment), referred to here as RTG, employed the 0.5° RTG SST product for lower boundary forcing over the ocean. The second experiment, referred to as MODIS, was identical the RTG in every way, except that the 1-km MODIS SST composite was used in place of the RTG SST analysis. The experiment design, in part, was chosen so as to allow the atmospheric boundary layer to adjust to the underlying sea surface prior to the forecast period. An intermittent data assimilation (IDA) cycle was implemented over a 3-h window prior to the forecast. Albeit somewhat short, the 3-h window is consistent with previous mesoscale modeling studies (e.g., Xue and Martin 2006; Dawson and Xue 2006). The IDA is launched at 2100 UTC, using the RUC-20 as a first guess, and the assimilated observations are described in section 3a. Because the RTG analysis is used within the suite of NCEP operational models (both the RUC-20 and Eta Model are initialized with the RTG), any adjustments in response to the lower boundary will manifest in the MODIS simulations only. Regardless, it is worth pointing out that the upwind marine boundary layer is continuously adjusting to SST variations. Lateral boundary conditions (LBCs) for the 3-h WRF simulation ending at 0000 UTC were derived from RUC analyses. The 3-h WRF forecast was then used as the background field for a second ADAS cycle at 0000 UTC to create the initial conditions for the subsequent 24-h forecast. The 0000 UTC ADAS analysis ensures that the initial conditions of the RTG and MODIS experiments are comparable where observations exist. The LBCs for the 24-h forecast period were obtained from the 40-km NCEP Eta Model grids at 3-hourly intervals. The MODIS composites used were obtained from the afternoon *Aqua* pass and were valid at approximately 1900 UTC daily. The SST fields were static during the 3-h assimilation and 24-h forecast periods. With the exception of the SSTs, both the RTG and MODIS runs are identical. To avoid the negative impact of spurious convection, which can promote significant error growth in short-term deterministic mesoscale forecasts (e.g., Zhang et al. 2006), we intentionally avoid the continuous/sequential data assimilation approach (Lorenc 1995) whereby the prior 24-h forecast is used to initialize the next cycle.

4. Results

One of the chief advantages of using the MODIS high-resolution SST fields in numerical weather prediction is the representation of mesoscale structures. Therefore, emphasis is placed on examination of the MABL structures in regions where strong SST gradients were found to exist, such as with the Florida Current and shelf waters (Fig. 2). Previous studies have shown that the MABL responds to flow across SST gradients (e.g., Song et al. 2004; O'Neill et al. 2005; Tokinaga et al. 2005).

Results from individual daily simulations will be presented. However, the most relevant impacts of the SST gradients were obtained by stratification of simulations according to the direction of low-level flow across the gradient, as discussed above. May 2004 included 10 easterly and 4 westerly flow cases, accounting for half of all of the simulations for the month. This a priori selection of regimes grouped together simulations in which the surface winds have a large normal component to the SST gradient along the western boundary of the Florida Current. Low-level gradient parallel flow did occur along portions of this SST gradient during portions of the simulations, and, in previous studies, has been shown to be beneficial to the enhancement of a solenoidal circulation between the cool and warm waters (e.g., Li et al. 2004). To isolate the impacts associated with the relatively quiescent nocturnal period, nighttime aggregates were composited by averaging hourly WRF output between 0500 and 1100 UTC. Additionally, a nine-point spatial smoother is applied to the output to isolate the mesoscale signal from smaller-scale noise.

a. Overview of simulation differences

Prior to discussing the aggregate results, a summary of some of the relevant differences between the model simulations is briefly presented here. Substantial differences in sea-breeze strength and onset time were not observed in the simulations, despite the fact that MODIS SST has significantly more detail. However, this is not surprising because the primary forcing mechanism for the sea-breeze circulation is associated with diurnal heating of the land surface, which is essentially identical for both the RTG and MODIS experiments. The MODIS simulations generated an earlier onset and greater amount of turbulent structure such as horizontal convective rolls (HCRs) over the marine area. Daily accumulated precipitation over the full domain was enhanced in the MODIS simulations by 5.9% over the entire month of May 2004. Subsections of the grid produced more dramatic differences. In an area defined

from the Bahamas, west to the Florida Straits, the precipitation increased by 11.7%, while in an area along the Florida Current precipitation increased by 27.3% for these MODIS cases.

Extended surface convergence zones, such as that associated with the Gulf Stream atmospheric front noted by Li et al. (2004), are observable in a few of the model runs. Figure 4 illustrates an example in which the 12-h MODIS simulation, valid at 1200 UTC 6 May 2004, produces elongated convergence zones over both the Florida Current and the transition zone between the Florida Current and the Florida–Hatteras shelf. Although on this particular day only one of the convergence zones appears to be associated with a cumulus cloud line, these features are typical of those observed in this region and are often precursors to deep convection, especially nocturnally (e.g., Lericos et al. 2002). The WRF simulations for 16 May 2004 develop convection early in the forecast period along two different boundaries. The RTG develops convection along the east-central Florida coast where convergence occurs (Figs. 5a,c). In contrast, the MODIS simulation develops convection to the east of this location along the significant SST gradient that is captured in the high-resolution SST product (Figs. 5b,d). Radar and visible satellite data (not shown) indicate that a line of convection developed west and downwind of the Bahamas, and streamed into the Florida peninsula just to the south of the noted convection in the WRF simulations. While neither model run captures this area of convection successfully, the change in location of the model precipitation from along the coast to just offshore is significant from an operational perspective. Additionally, the impact illustrates the sensitivity of the WRF to high-resolution SSTs. For this particular event, the SST specification appears to be a secondary issue as the mesoscale forcing associated with the generation of precipitating cloud systems over and downwind of the Bahamas dominates. Enhanced low-level convergence and precipitation, formed along the SST gradient in the MODIS simulations, are commonly observed over the coastal waters of this region and are visible as cloud lines in both radar and satellite images.

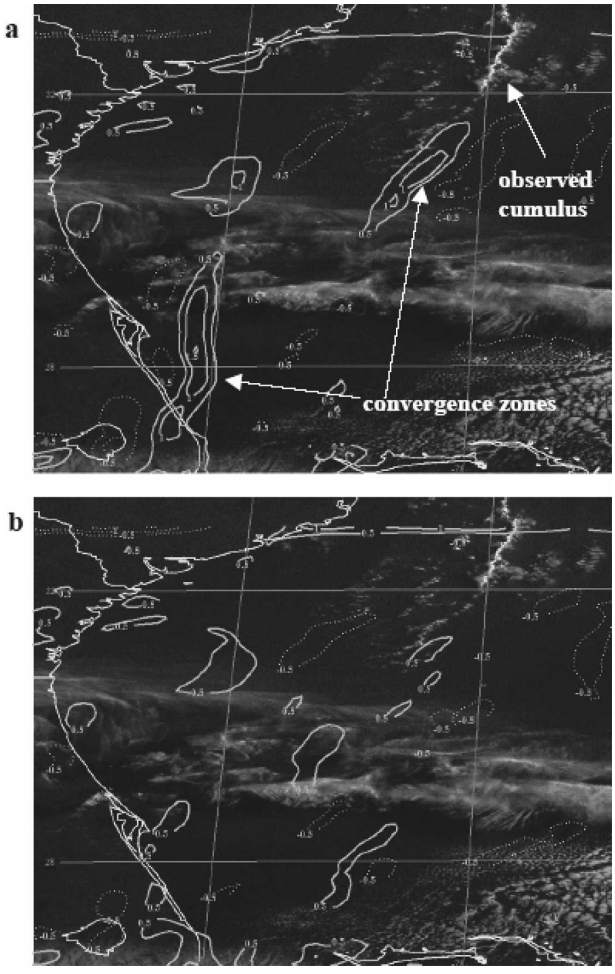

FIG. 4. Visible GOES image from 1130 UTC 6 May 2004 with WRF surface convergence (contours, every 0.5 $s^{-1} \times 10^6$) at 1200 UTC (12-h forecast) for (a) MODIS and (b) RTG. A line of congested cumulus in the northeast portion of the domain coincides with an elongated zone of convergence in the MODIS simulation, while a second convergence zone along the Florida–Hatteras shelf was not associated with low-level cloud development. The RTG does not produce significant convergence.

b. Easterly and westerly flow regimes

As previously discussed, aspects of the MODIS SST impact for specific wind regimes are more easily discerned with composite statistics. Aggregate 10-m wind for both the easterly and westerly flow regimes are shown for the nocturnal period in Fig. 6. Differences in the wind direction between the two regimes are most significant over the northern portions of the domain, especially along the Florida Current. The focus is on the waters off the eastern coast of Florida where easterly (westerly) flow is associated with the transit of air parcels from (to) the warm Florida Current waters to (from) the cooler shelf waters. The following results are based on the easterly and westerly regime specifications.

1) SURFACE AND INTEGRATED FIELDS

(i) Surface fluxes

In a related study, Rouault et al. (2003) noted relatively significant errors in simulated latent and sensible heat fluxes over the Agulhas Current, a western bound-

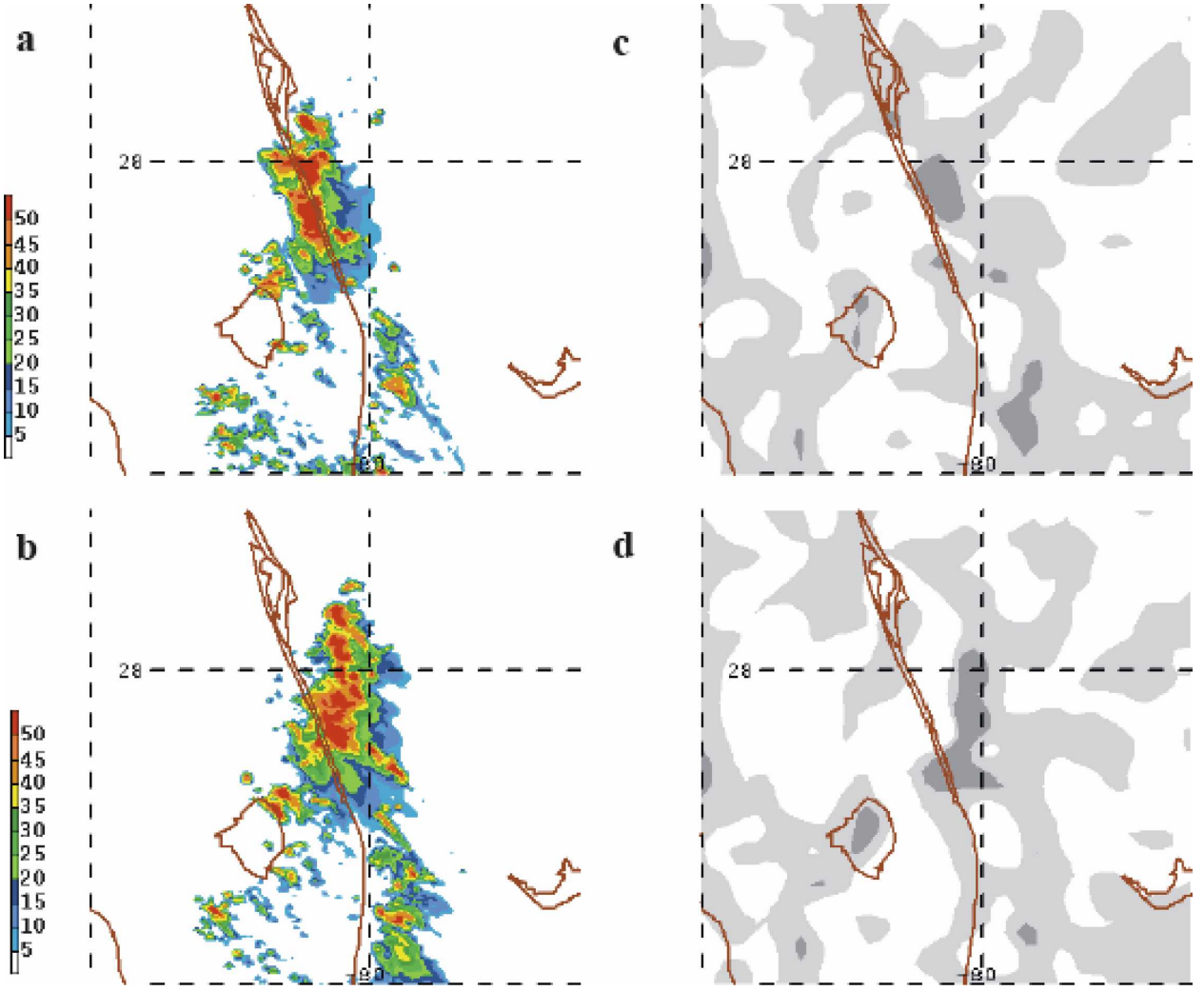

FIG. 5. Model reflectivity (dBZ) 3-h forecast valid at 0300 UTC 16 May 2004 for (a) RTG, (b) MODIS; model convergence, spatially filtered and smoothed (shaded for values greater than 2 and 4 $s^{-1} \times 10^{-4}$) for (c) RTG and (d) MODIS. The RTG simulation produces thunderstorms along the coastal convergence zone, while the MODIS simulation generates convection along a convergence zone on the western edge of the Florida Current close to 80.0°W.

ary current near Africa that has sharp SST gradients. These errors were in part shown to be related to the use of low-resolution SST products. A comparison between the two SST products used herein is shown in Fig. 7, depicting the average SST differences (MODIS − RTG) for the easterly and westerly flow regimes. Positive differences in SST (where the MODIS SST composite is warmer) along the Florida Current, for example, indicate where the MODIS SST product better captures the higher-resolution detail. The westerly flow regime shows negative differences, which are clearly more confined to the near-coastal region than in the easterly flow regime. This may be attributed to upwelling in the inner shelf. For brevity, the differences in surface sensible and latent heat fluxes are shown for the nocturnal easterly flow cases only (Figs. 8 and 9, respectively). Positive (negative) differences in SST are associated with increased (decreased) surface sensible and latent heat fluxes. Sensible heat fluxes increased in the MODIS runs by as much as 100% in the Florida Current, while latent heat flux increases approached 30%. These differences provide an initial indication that the WRF is sensitive to the high-resolution SSTs.

(ii) Mean sea level pressure

Differences in the sensible and latent heat fluxes should impact the evolution of other state and kinematic fields. For example, Tijm et al. (1999) have shown that the pressure field responds to changes in the surface fluxes between land and ocean associated with the

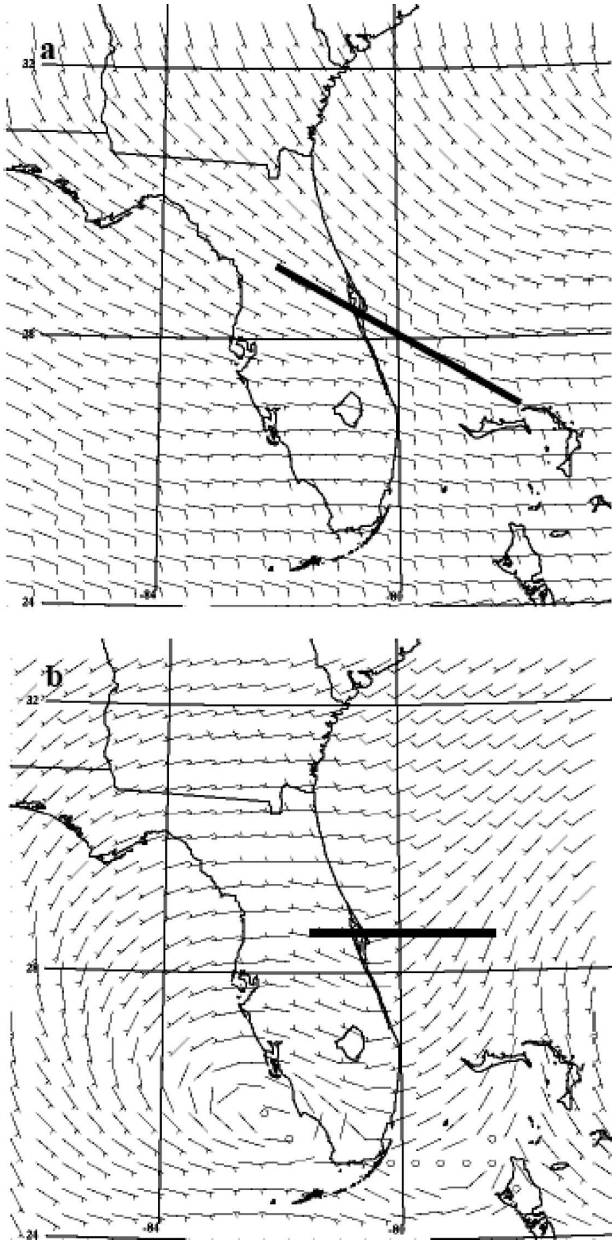

FIG. 6. Nocturnal mean 10-m wind speed and direction (m s^{-1}) for (a) easterly and (b) westerly wind regimes during May 2004. The solid black lines in (a) and (b) represent the axes of the cross sections shown in Fig. 19.

sea breeze. Here, the largest impact on the sea level pressure (SLP) field is simulated to be downwind of the significant changes in the surface heat flux, especially in the vicinity of the Florida Current and the Bahamas. The easterly flow regime shows two distinct regions in which the MODIS simulations produce lower SLP: over southeast Florida and off the Florida northeast coast just west of 80.0°W (Fig. 10a). In contrast, for the westerly flow cases, the two negative pressure anomalies are shifted eastward (Fig. 10b). The different responses in SLP between the two regimes illustrates the importance of flow-dependent (i.e., advective) effects that act to displace the response downstream of the forcing. The use of the MODIS SST composite produced changes in average sea level pressure of up to 8 Pa, which are on the order of that observed with mesoscale phenomena, such as sea or lake breezes.

(iii) Kinematics

The impact on the surface wind field in response to the pressure forcing (i.e., changes in the pressure gradient) has been documented in other studies (e.g., Lindzen and Nigam 1987). The pressure gradient model is analogous to the sea-breeze circulation, whereby changes in SSTs lead to a change in surface fluxes and a subsequent thermal response in the MABL. Warmer (cooler) SSTs lead to lower (higher) sea level pressure, thereby modifying the pressure gradient and producing surface wind accelerations (decelerations). In an alternative model, changes in the MABL stability (and thus vertical wind stress divergence) across an SST gradient induce surface wind accelerations (e.g., Wallace et al. 1989; Koračin and Rogers 1990). The transit of air parcels across SST gradients has been investigated in this context (Song et al. 2004; Song et al. 2006; Nonaka and Xie 2003). It has been shown to impact the flow differently for parcel trajectories moving parallel to the temperature gradient (Samelson et al. 2006). In particular, Samelson et al. (2006) show that the wind and temperature profiles reflect a well-mixed layer over warm SSTs. In this case, a warming of SSTs leads to a less stable MABL. This causes both an increase in mixing and a higher surface stress (but decreased vertical wind stress divergence), which is reflected by faster winds near the surface. Additionally, past studies have shown that models tend to underestimate the relationship between the wind stress and SST, especially in regions of significant gradients (Maloney and Chelton 2006).

The two mechanisms discussed previously are referred to here as follows: 1) *vertical wind stress divergence* (parcel wind speed changes associated with stability changes within the surface layer and/or a shallow internal boundary layer; e.g., advection of warm air over cooler waters) and 2) *pressure gradient forcing* (parcel accelerations resulting from the modification of the pressure gradient). The comparison of the MODIS and RTG runs pressure fields will be referred to as *perturbation pressure gradient forcing*. For the easterly flow regime, surface air parcels pass over the warm Florida Current to the cooler shelf waters with the expectation that parcel deceleration may be caused by either forcing mechanism—(a) an increased vertical

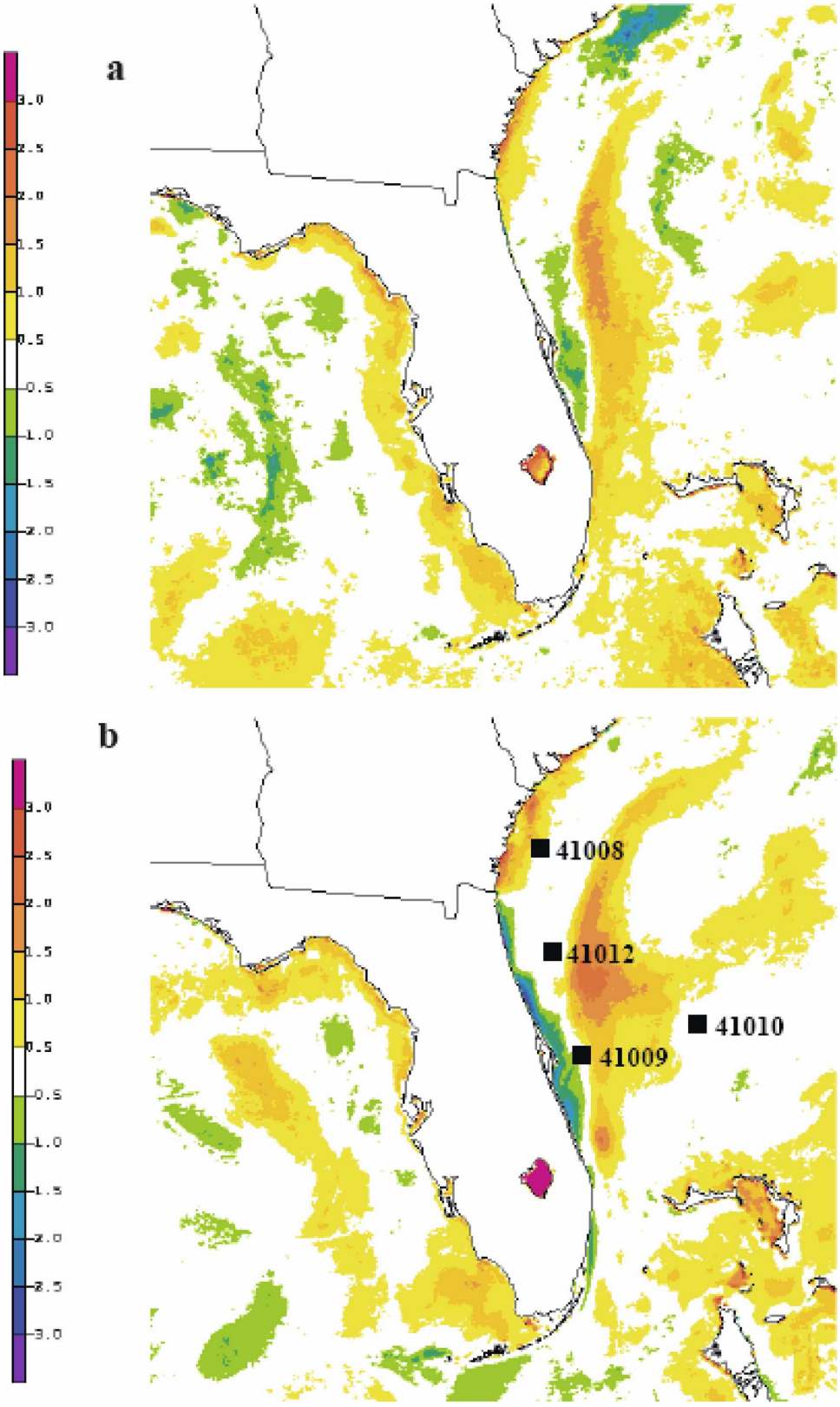

FIG. 7. May 2004 mean SST differences (MODIS − RTG; K) for (a) easterly and (b) westerly flow regimes. Black squares on (b) indicate locations of buoys used for model verification.

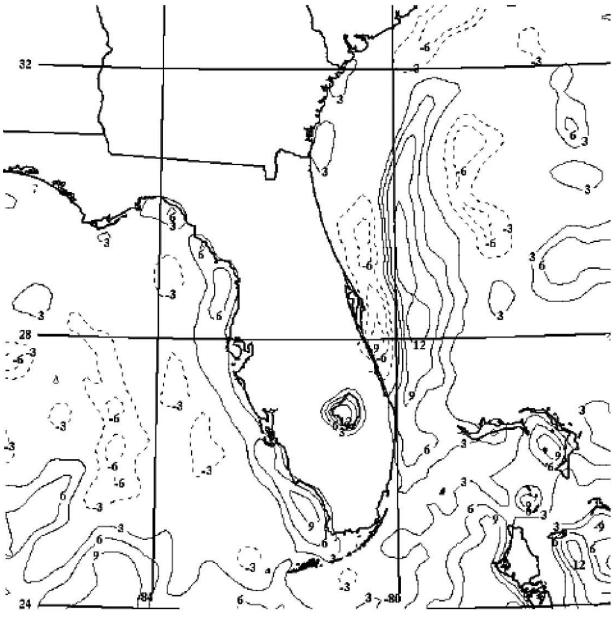

FIG. 8. Average difference in surface sensible heat flux (W m^{-2}) between MODIS and RTG runs for nocturnal easterly-flow cases.

wind stress divergence within the enhanced stability of the cooler shelf waters or (b) the eastward-pointed perturbation pressure gradient in that region (Fig. 10a). Figure 11 depicts the impact of the MODIS SST composites on the simulated 10-m winds and shows decelerating (accelerating) flow across the enhanced SST

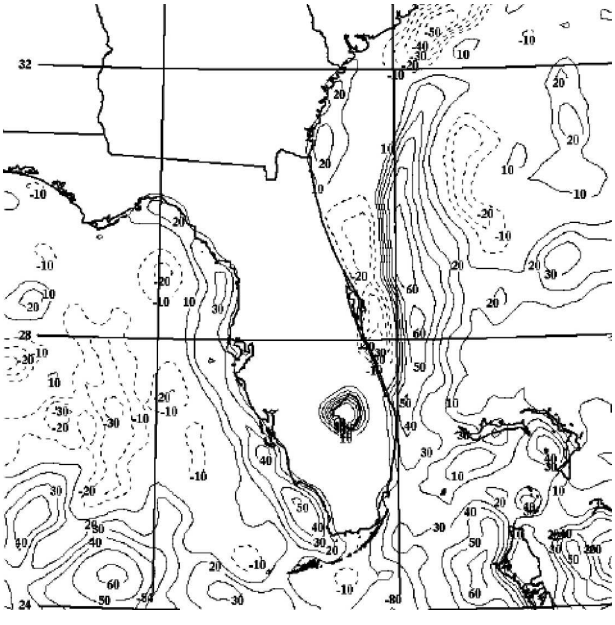

FIG. 9. As in Fig. 8, but for surface latent heat flux difference (W m^{-2}).

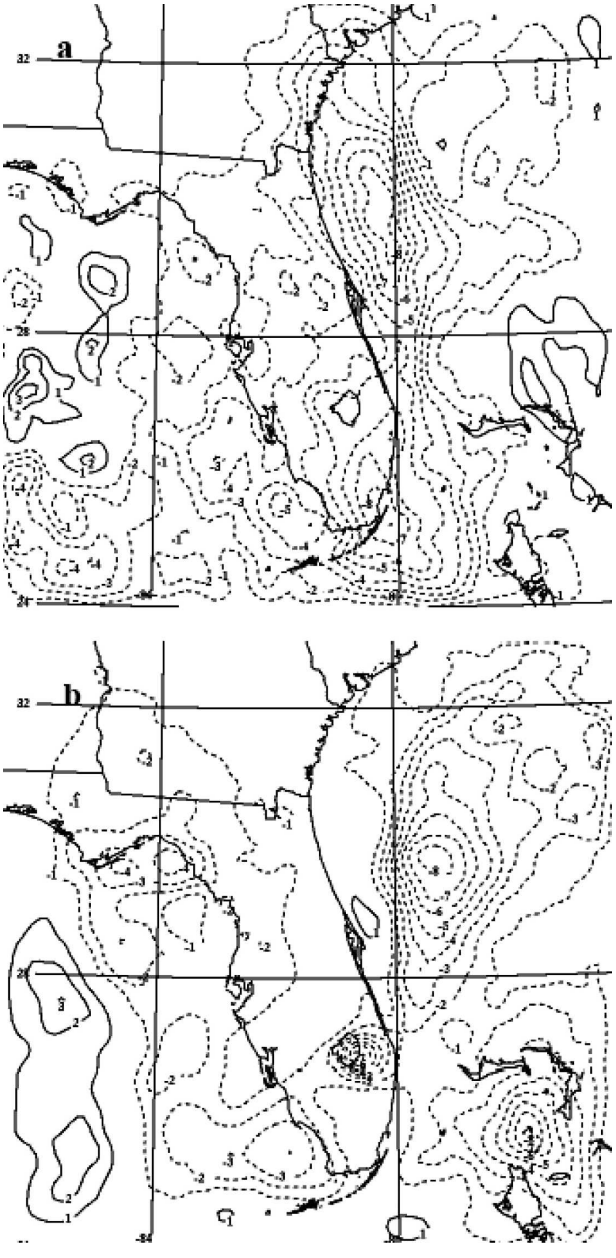

FIG. 10. As in Fig. 8, but for mean sea level pressure difference (Pa) for (a) easterly- and (b) westerly-flow regimes.

gradient under easterly (westerly) flow regimes consistent with either forcing mechanism. While the perturbation pressure gradient forcing is consistent with the modeled deceleration for the easterly-flow case, it would be expected to lead to a larger acceleration (and hence a more positive wind difference than that observed) east of the perturbation pressure gradient minimum (gray box in Fig. 11a). In fact, there is only weak acceleration in this region (Fig. 11a). To better understand the acceleration differences, the various forcing

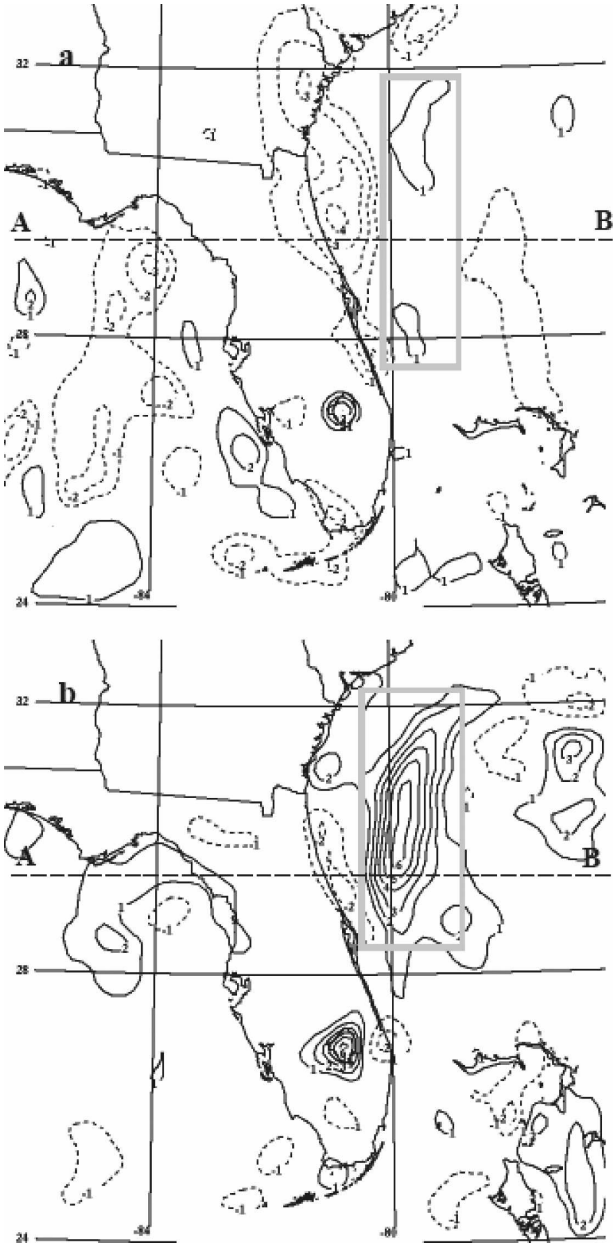

FIG. 11. As in Fig. 8, but for nocturnal average 10-m wind speed difference ($m\ s^{-1} \times 10$) for (a) easterly- and (b) westerly-flow regimes. Dashed line segment AB delineates the cross-sectional transect shown in Figs. 17 and 20. See text for discussion related to gray boxes.

components (i.e., pressure gradient force, Coriolis force, and vertical winds stress divergence) were calculated (Fig. 12). The vertical wind stress divergence was calculated as a residual acceleration because the WRF does not explicitly output this acceleration for the surface. For the easterly flow cases, the perturbation pressure gradient force acts to accelerate the wind, while the vertical wind stress divergence generally works to decelerate the flow in this region (gray box, Fig. 12a). Conversely, for westerly flow, the vertical wind stress divergence overwhelms the pressure forcing in the region of significant positive wind differences (gray boxes, Figs. 11b and 12b). For these cases, very stable low-level air is advecting off the Florida peninsula [see section 4b(2)], thereby limiting the depth of the vertical response. Although the largest perturbation pressure gradient vectors are in the northeast portion of the domain (Fig. 12b), these tend to oppose the stress divergence vector, thereby mitigating the impact on the wind differences (note the smaller secondary positive wind difference to the northeast of the main signal in Fig. 11b). Furthermore, these large perturbation pressure gradient vectors are an artifact of convection, which overwhelms the more subtle mesoscale signal responsible for the wind differences shown in Fig. 11 (not shown). The response to the high-resolution SSTs is flow dependent, with about twice as much response in the wind speed along parcel trajectories that transition from cool to warm. Wind speed changes between MODIS and RTG runs are on the order of 6% (9%) in the westerly (easterly) flow regime in the vicinity of the Florida Current (not shown). Qualitatively, the impact of the high-resolution SST product in the WRF model produced changes in the wind field that are consistent with recent studies.

While the impact on the wind field is relevant, it is also instructive to evaluate changes in surface divergence because wind speed accelerations previously noted might be largely compensated for by directional changes to the wind. The response of this derived field for May 2004 is also flow dependent, with an increase in convergence to the west of the significant SST gradient (associated with the west side of the Florida Current) for the nocturnal easterly flow cases (Fig. 13a). A convergence zone associated with the western edge of the Gulf Stream has been noted by Raman et al. (1998) to be associated with a coastal front; however, that case consisted of a significant synoptic-scale temperature gradient and trough. Here, convergence axes shifted to the east of the SST gradient for westerly flow cases (Fig. 13b), with the changes in convergence being a factor of 2 larger in magnitude and spatially more coherent than in the easterly flow cases. The accelerations in the surface winds introduced by the use of the MODIS SST produce changes to the surface divergence that are more pronounced in the SST gradient regions.

(iv) Boundary layer height

Changes in the depth of the mixed layer are anticipated as a result of the differences in the surface heat fluxes in the simulations. The WRF boundary layer

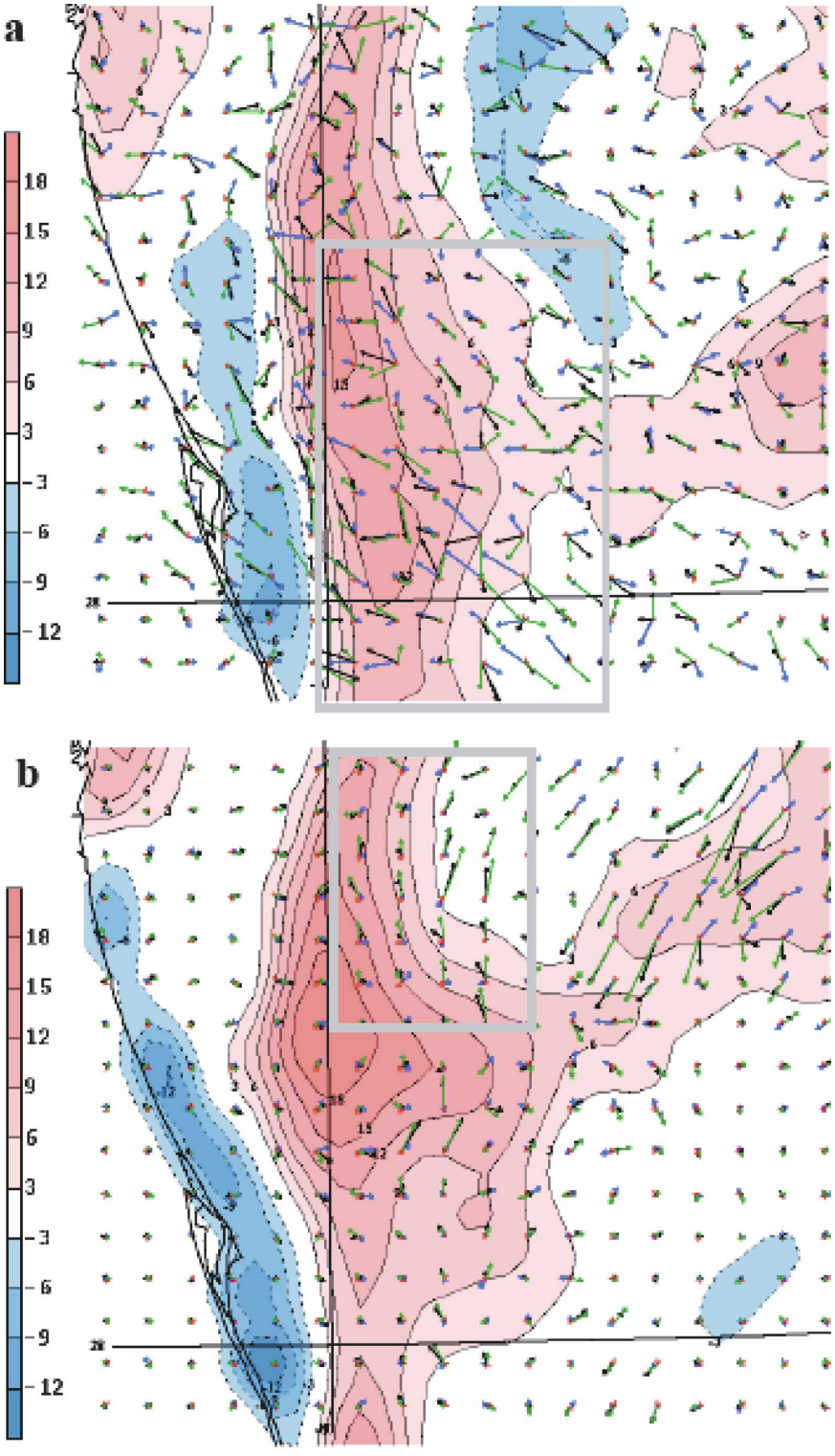

FIG. 12. MODIS − RTG simulated differences valid for nocturnal (a) easterly and (b) westerly cases. SSTs (color filled; K) and acceleration vectors for Coriolis (red), pressure gradient force (blue), vertical wind stress divergence (green), and 10-m parcel (black). See text for information regarding the gray boxes. Vectors in (b) are scaled by a factor of one-half.

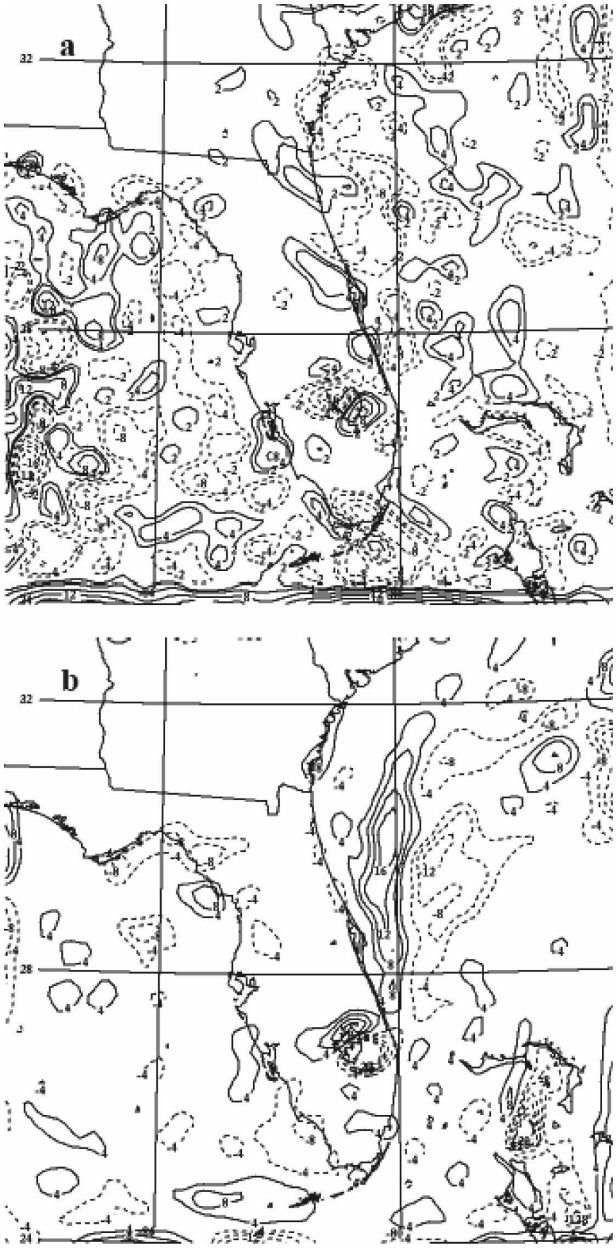

FIG. 13. As in Fig. 8, but for mean divergence ($s^{-1} \times 10^6$) difference for (a) easterly- and (b) westerly-flow regimes.

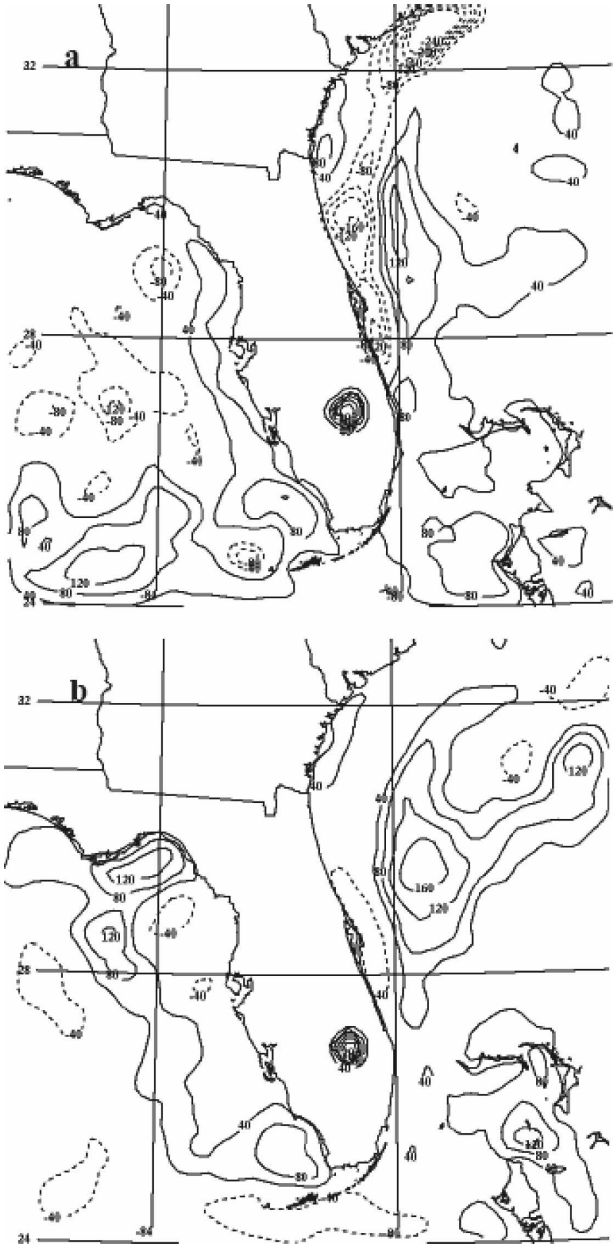

FIG. 14. As in Fig. 8, but for mean planetary boundary layer height difference (m) for (a) easterly- and (b) westerly-flow regimes.

height is estimated using a bulk Richardson formulation (Troen and Mahrt 1986), which is dependent on near-surface conditions, with modifications that explicitly account for entrainment at the top of the mixed layer (Hong et al. 2006). Figure 14 illustrates the SST impact on the WRF estimates of the nocturnal boundary layer heights, which are lower (higher) in regions where the SSTs have cooled (warmed). The apparent impact over the cooler shelf waters is more pronounced in the easterly flow cases, a result that is consistent with the extended fetch associated with the southeasterly flow (Fig. 6a) and negative SST anomalies (Fig. 7a). Changes in the WRF boundary layer height estimates are primarily due to the influence of the underlying SSTs that impact the bulk Richardson number. A comparison between Fig. 8a (sensible heat flux difference) and Fig. 14a (PBL depth difference) indicates that the WRF PBL height differences are strongly driven by the changes in the sensible heat flux between the simula-

tions. The degree of impact is modulated by the low-level trajectories with significant differences evident between the easterly and westerly flow regimes. Changes in boundary layer depth in the regions of maximum SST differences (i.e., within the Florida Current) between the MODIS and RTG products are comparable to those reported by Rouault et al. (2000) for a study over the Agulhas Current, but less than that found by Tokinaga et al. (2006) in a wintertime observational study over the Kuroshio extension (east of Japan). Despite recent improvements in the WRF estimate of PBL height (Hong et al. 2006), potential ambiguities remain in its representation, and thus differences in the potential temperature and static stability are also shown in the following sections.

2) Vertical profiles and cross sections

(i) Potential temperature and static stability

Changes in the surface pressure fields as a result of the spatially varying SST forcing must be associated with vertical modification of the thermal and moisture fields. Figure 15a shows an east–west cross section of potential temperature along 28.5°N. The MODIS SST composite was found to have a significant impact on the nocturnal easterly-flow cases. The lower MABL-simulated potential temperature progressively increases in the MODIS experiment from east to west in a deepening layer with the greatest impact associated with the warmer MODIS SST within the Florida Current. Meanwhile, the upper MABL cools in response to rising motion associated with a progressively deeper MABL, a finding similar to that shown by Hashizume et al. (2002) for SST changes associated with tropical instability waves. The impact on the MABL thermal field is absent over the Florida peninsula, while a shallow layer of relative warming reappears in the MODIS run associated with warm near-coastal SSTs off of Florida's west coast.

Concurrent changes to atmospheric stability, assessed as $\partial \ln\theta(\partial p)^{-1}$, are shown in Fig. 16a. A stability difference couplet, located near the boundary layer top, is consistent with an increasing boundary layer height from east to west. A separate layer of decreased stability near 950 hPa lies just above regions in which the PBL has warmed. Small low-level stability increases are seen along the Florida–Hatteras shelf, where the MODIS SSTs are cooler than the RTG SSTs, through the layer from 975 hPa to the surface. Note that the drop in boundary layer height upon transition to the cooler shelf waters (Fig. 14a) does not appear to be associated with a change in the boundary layer top as viewed in Fig. 15a. This indicates that the PBL height changes are dominated by low-level changes in parcel surface buoyancy.

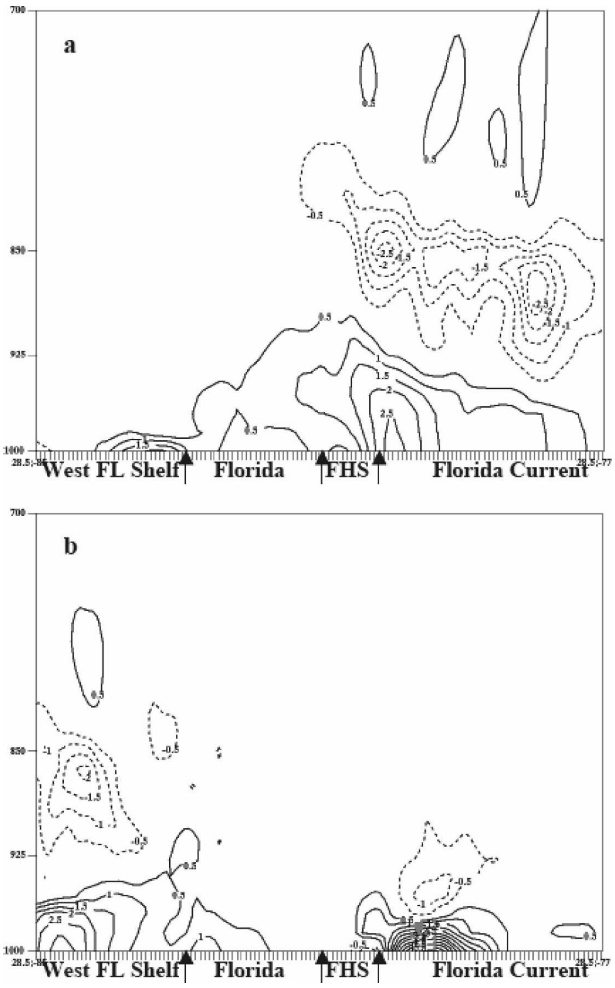

FIG. 15. Vertical cross section through entire domain along 28.5°N of difference in potential temperature (°C) between MODIS and RTG runs for nocturnal easterly flow cases. Maximum positive differences (solid contours) are associated with warmer MODIS SST over the Florida Current and west Florida shelf for (a) easterly- and (b) westerly-flow regimes.

Composite potential temperature profiles for the easterly flow cases are shown in Fig. 17a. The profiles, each separated by 1° of longitude, are taken along a west-to-east transect that samples the region with the largest 10-m wind impact (see Fig. 11). For easterly flow, the lower troposphere (below 1000 hPa) is unstable upstream (to the east) of the FC with comparable static stability in both simulations. The MODIS simulation temperatures are warmer however, consistent with the southeasterly flow and positive SST differences upstream (Figs. 6 and 7). In both runs, the atmosphere appears to be well mixed from about 1000 to 940

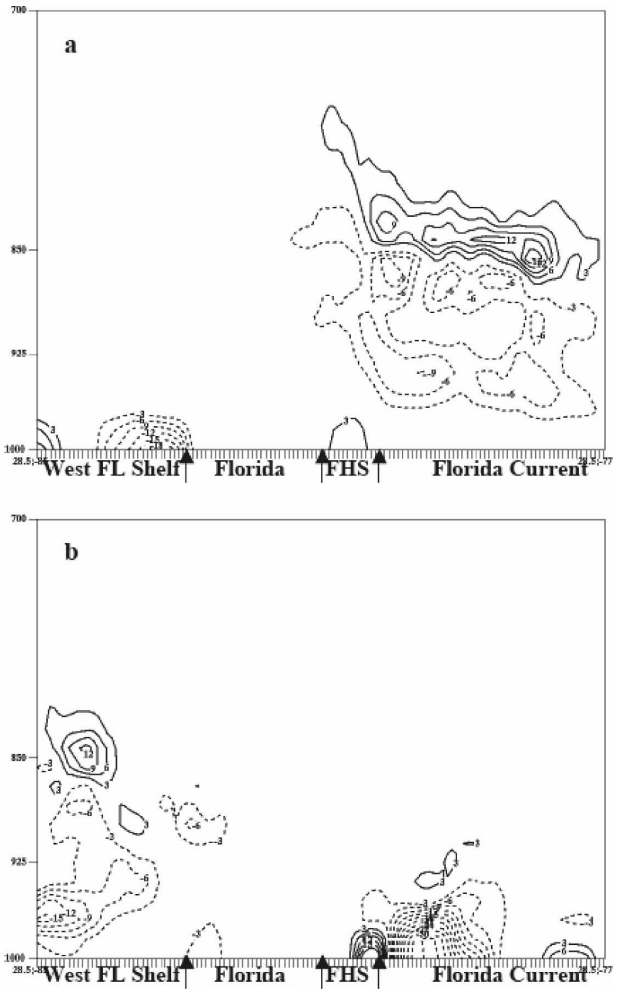

FIG. 16. As in Fig. 15, but for difference in $\partial \ln\theta(\partial p)^{-1}$ (°C Pa^{-1}) for (a) easterly- and (b) westerly-flow regimes.

hPa, with only small differences above 920 hPa. Temperature differences between the simulations increase over the FC with similar static stability above the surface layer (from 1000 to 940 hPa). Both profiles remain unstable below 1000 hPa, however the lapse rates are steeper in the MODIS simulations. There are relatively significant changes in the stability of the easterly flow cases as air traverses the cooler shelf water, with lapse rates increasing and becoming stable below 1000 hPa. Again, the MODIS temperature profile is slightly warmer. Across front potential temperature differences are about twice that between simulations.

The impact on the thermal field in the westerly flow cases (from cool-to-warm waters) along 28.5°N differs significantly compared to the easterly flow cases off of Florida's east coast. Very slight cooling is noted over the Florida–Hatteras shelf in the MODIS run, while strong but shallow warming occurs over the Florida Current (Fig. 15b). Stability changes are also more shallow and intense than in the easterly flow cases (Fig. 16b). For example, the relative stability increase for parcels moving over the Florida–Hatteras shelf in the MODIS runs are nearly an order of magnitude larger than in the easterly flow cases. As air flows over the Florida Current, the stability changes are also seen to be higher in magnitude and shallower in depth. Some of the differences between the nocturnal flow regimes probably arise from parcel trajectory differences, because the surface parcels that reach cool shelf waters have a stable history over land in the westerly flow cases, thus leading to relatively nominal changes in temperature and stability over the Florida–Hatteras shelf. Angevine et al. (2006) have shown that model stability in coastal waters (in a transition from warm land to cool waters) was significantly weaker than the observed stability. This discrepancy was attributed to common problems with modeling of the stable boundary layer. In another related study of warm offshore flow over cool coastal waters, Skyllingstad et al. (2005) compared mesoscale and large-eddy simulation model output to observations. They also found that the models had difficulty with the boundary layer in this situation. Consequently, the results presented here should be interpreted with these caveats.

For the westerly-flow cases (Fig. 17b), the upstream (over the FHS) MODIS temperature profile is cooler and more stable below 1000 hPa as the lower tropospheric air traverses the negative SST differences in the near shore (Fig. 7b). Above 1000 hPa, the differences between the model runs are small in this region. Over the FC, below 1000 hPa, the MODIS simulations transition to being slightly unstable while the RTG remains stable. The MODIS simulation temperatures are warmer (up to about 980 hPa) than the RTG, the latter of which has no discernible added heat content. Downstream (to the east) of the FC, MODIS has a deeper mixed layer.

(ii) Kinematics

Above the lowest model level, *a prognostic PBL momentum exchange* replaces the diagnostic surface parameterization scheme. Vertical exchange is accomplished through eddies ranging from the subgrid to the resolvable grid scales. While the SST impact on the 10-m wind appears to be dominated by changes in both the surface layer vertical wind stress divergence and the pressure gradient, PBL momentum exchange is generally much smaller in magnitude than the pressure gradient forcing throughout the marine PBL (Fig. 18). The difference in nocturnal wind speed between the MODIS and RTG simulations, taken along the transect

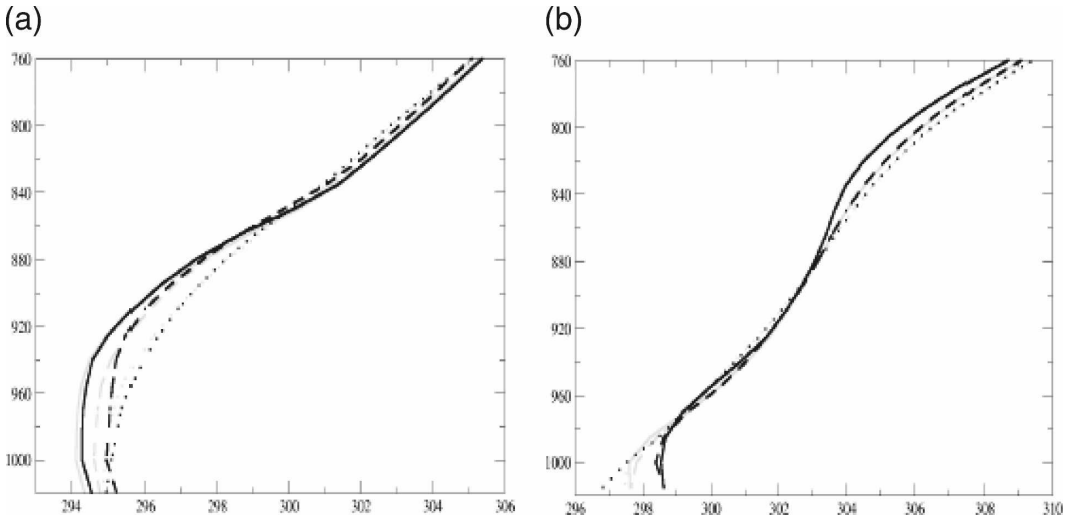

FIG. 17. Nocturnal (0500–1100 UTC) potential temperature (K) profiles for MODIS WRF (black) and RTG WRF (gray) along 29.5°N, at 79.0° (solid line), 80.0° (dashed line), and 81.0°W (dotted line) for the (a) easterly-flow and (b) westerly-flow regimes.

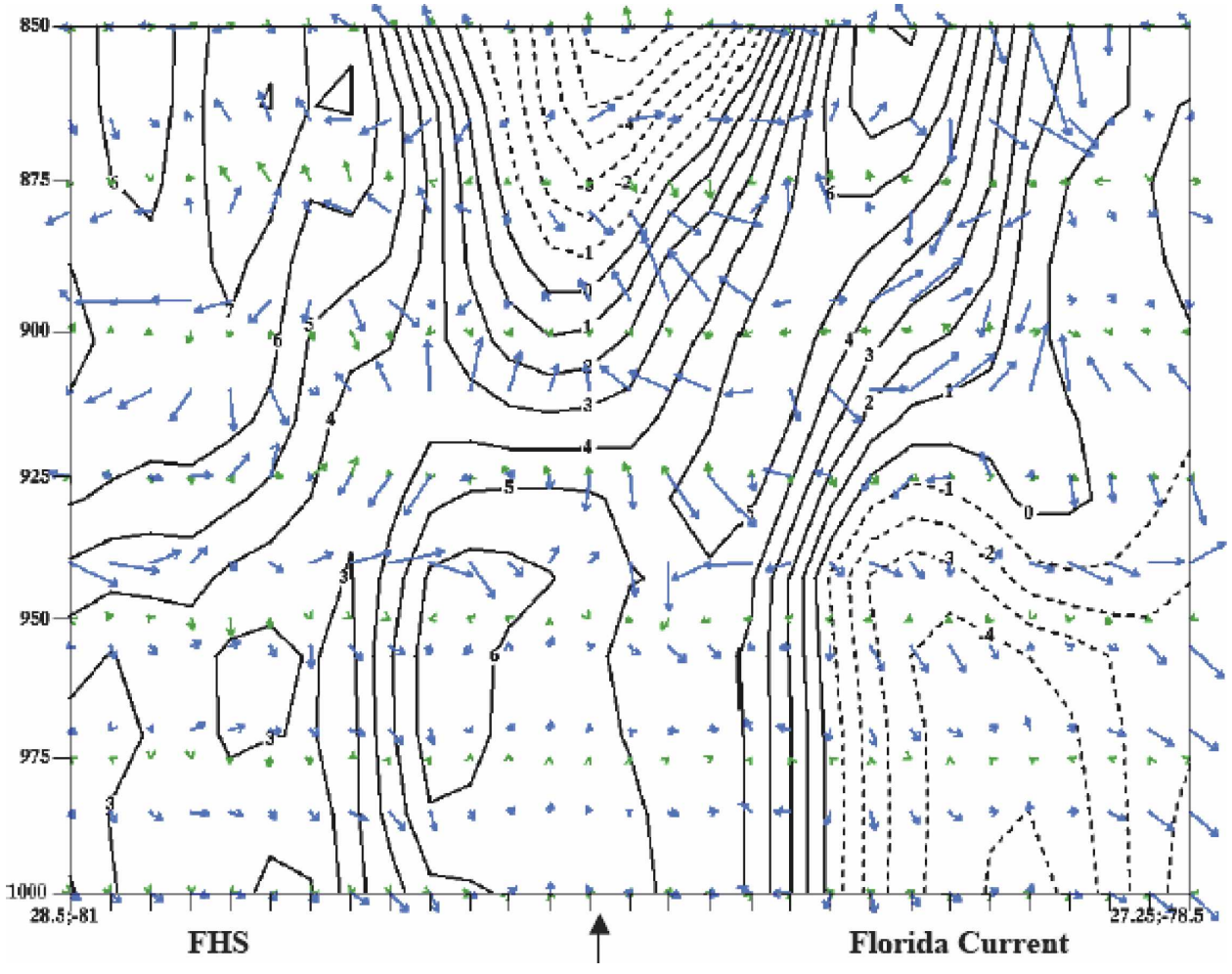

FIG. 18. Northwest-to-southeast vertical cross section for 16 May 2004 mean wind speed difference (contours; m s^{-1} × 10) and acceleration vectors: pressure gradient force (blue) and vertical wind stress divergence (green).

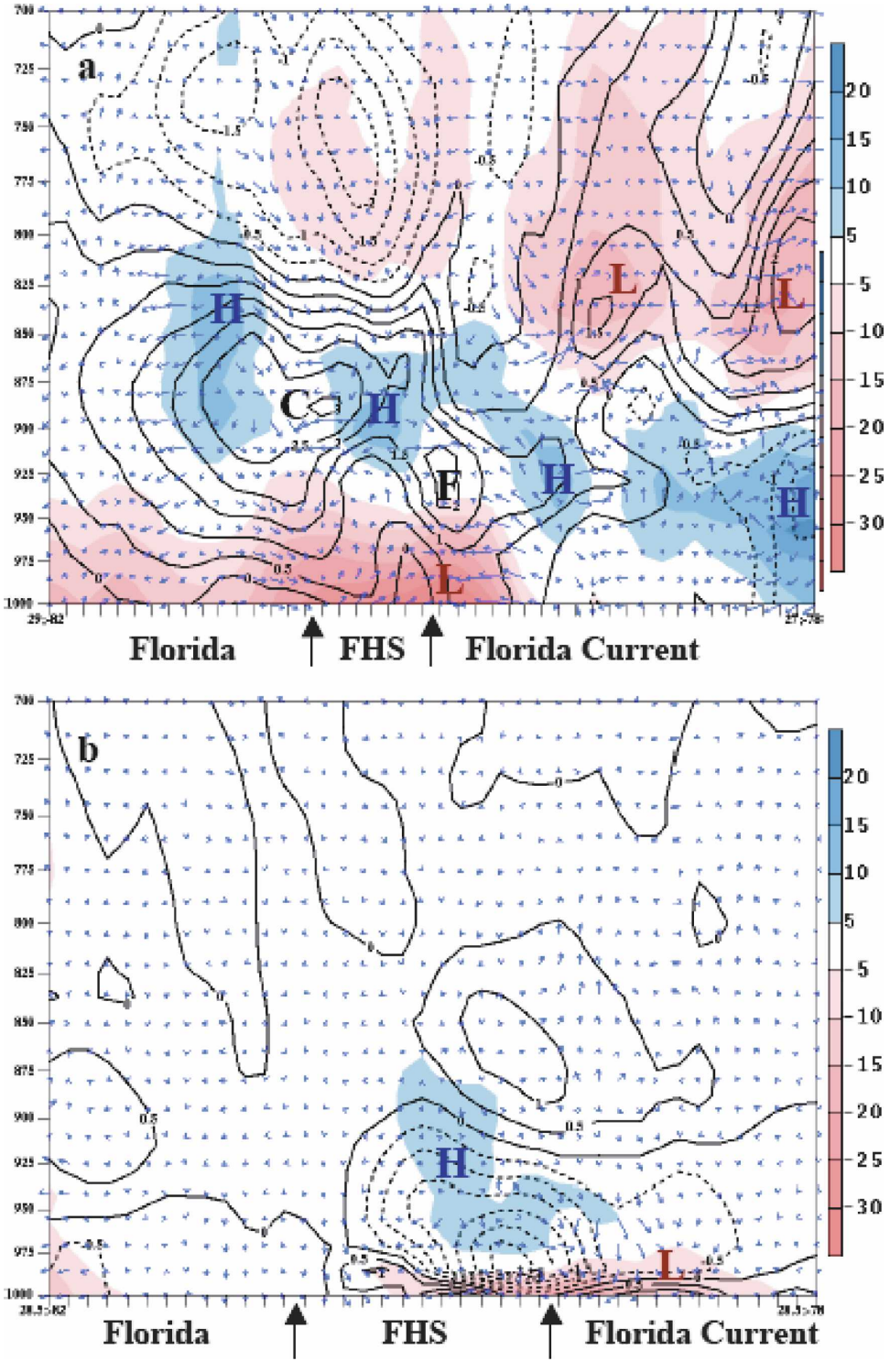

FIG. 19. Vertical cross section of mean wind speed difference (contours; m $s^{-1} \times 10$), height difference (shaded; m), and perturbation pressure gradient force (vectors) for (a) easterly- and (b) westerly-flow regimes as shown on Fig. 6. Regions of high and low height differences are indicated with a blue H and a red L, respectively. The maximum wind difference along the coast is indicated by a black C and the maximum wind difference within the Florida Current is annotated with a black F on (a) above.

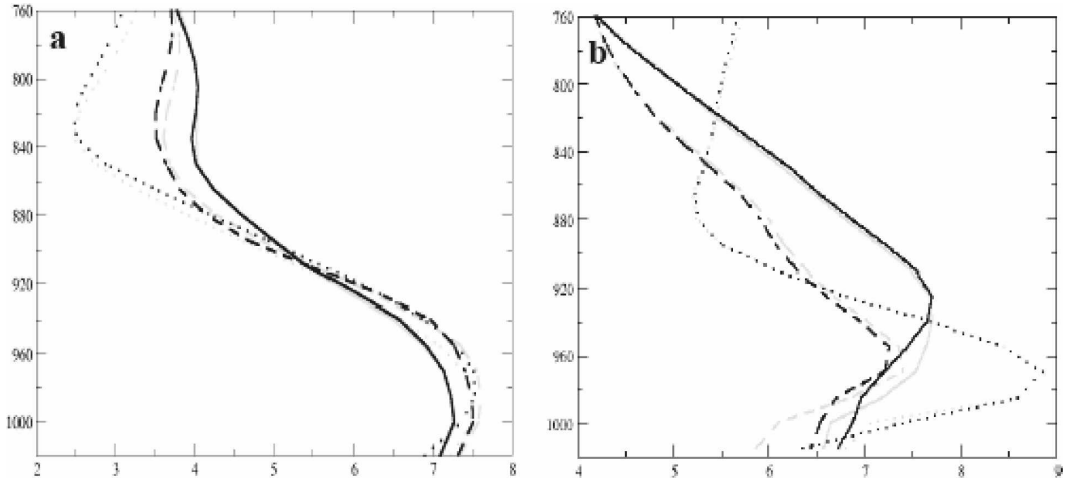

FIG. 20. As in Fig. 17, but for composite wind profiles (m s^{-1}).

shown in Fig. 6a, for the easterly-flow cases shows a significant vertical structure (Fig. 19a). Most notable is the wind speed increase in the MODIS run, which increases in depth from about 50 hPa above the Florida Current to approximately 150 hPa over Florida's east coast. This wind speed increase is driven primarily by the perturbation pressure field, the latter of which is a direct response to the thermal forcing in this region (the Florida Current). The wind field response is also consistent with height field changes (Fig. 19). The wind speed increase is not a result of momentum transfer because the mean wind profile for the easterly flow cases indicates that winds are decreasing with height in this region (Fig. 20a). Hashizume et al. (2002) have also noted a similar scenario in the eastern equatorial Pacific where the wind profile, perhaps due to seasonal variations, was opposite to that necessary for the PBL momentum exchange to decrease winds. Modulations in the increasing wind region are seen, for example, over the Florida–Hatteras shelf east of the wind difference maximum (F in Fig. 19a). The deceleration of the wind is associated with an opposing perturbation pressure gradient to the east of a perturbation pressure ridge. Pressure gradient perturbations are the forcings that are primarily responsible for the significant variations in the wind difference field over the nocturnal marine boundary layer.

Composite wind profiles for the easterly flow cases are shown in Fig. 20a at the same locations as for the composite temperature profiles. Upstream (to the east) of the FC the wind profiles are nearly identical for both model runs, with a low-level wind maximum at 1000 hPa. Over the FC, both the RTG and MODIS low-level (below 900 hPa) winds increase, with the RTG winds being slightly larger. Above 900 hPa, the reverse occurs, that is, the winds decelerate for both runs. The most significant wind differences occur downstream of the FC (over the FHS) in association with large negative SST differences. The impact to the wind speeds along the same cross section for the westerly flow cases is very limited (Fig. 19b) in its vertical extent (resultant from the large enhanced stability in the westerly flow regime). The negative wind difference maximum that dominates the marine PBL is associated with a perturbation pressure ridge axis.

For the westerly flow cases, the composite wind profiles are more variable (Fig. 20b). Over the FHS, the impact is confined to below 1000 hPa, with greater shear in the MODIS simulations, and is concomitant with the increased stability (Fig. 17b). Both sets of model runs exhibit a coastal wind maximum near 970 hPa, which decrease in amplitude and increase in height downstream. The largest of the wind differences, between simulations, occurs over the FC below 980 hPa, again corresponding to the marked low-level stability changes (Fig. 17b). There is reduced vertical shear, between the level of maximum winds and the surface, in the MODIS simulations both over and downstream of the FC.

3) VALIDATION

Heretofore, the results shown have focused on the SST impact via comparison of simulations using two distinct model lower boundary conditions. The emphasis here is on model validation, where possible. Although data are limited over the marine boundary layer east of the Florida peninsula, the National Data Buoy Center (NDBC) buoy data with collocated WRF model output were compared (Table 1). Buoy wind speed estimates were adjusted to the 10-m level following Hsu

TABLE 1. Comparison of composite WRF simulations with NDBC buoy wind speeds and wind speeds adjusted to a 10-m height for easterly- (westerly-) flow regimes. Boldface values indicate the simulation that compared best to the 10-m wind speed estimates.

NDBC buoy	Location	Buoy avg wind speed ($m\ s^{-1}$)	Buoy avg wind speed at 10 m ($m\ s^{-1}$)	RTG SST wind speed	MODIS SST wind speed
41008	31.40°N, 80.87°W	4.05 (6.45)	4.37 (6.97)	5.86 **(8.17)**	**5.82** (8.28)
41009	28.50°N, 80.17°W	6.74 (4.33)	7.27 (4.67)	7.54 (4.80)	**7.46** (**4.70**)
41010	28.95°N, 78.47°W	7.00 (4.82)	7.56 (5.21)	6.64 (5.01)	**6.69** (**5.08**)
41012	30.00°N, 80.60°W	5.07 (5.14)	5.48 (5.55)	6.91 (6.41)	**6.64** (6.41)

et al. (1994). Both the RTG and MODIS experiments tend to overpredict 10-m wind speeds with the poorest performance found at buoy 41008. The use of the MODIS SSTs led to a slight reduction in error. Analysis of these data by hour shows that the wind speed bias within WRF varies diurnally as well as regionally (Fig. 21).

Simulated 10-m wind speeds were also compared with remotely sensed data from the 37-GHz channel on the TMI. The 37-GHz channel has a smaller footprint than other available channels, and will thus better resolve winds near coastal areas (M. Brewer 2006, personal communication). For the easterly-flow cases, there is a general agreement between TMI wind speed and the MODIS simulations (e.g., weaker winds over the west Florida shelf); however, there are also significant differences (Fig. 22). In particular, a ridge of higher wind speeds seen in the MODIS run (hatched line in Fig. 22b) along the Florida Current is not present in the TMI data. This finding is consistent with the positive bias in the WRF surface layer winds over the Florida Current as seen in the comparison with buoy 41009. Because a similar bias was also observed in the RTG run, the cause is not related to the SST specification in particular (not shown).

Comparison of the simulated and buoy 2-m air temperatures (Fig. 23) indicates that the model differences are smaller than the difference between the models and the buoys. During the night, the models show a similar cooling trend when compared to the buoys, however, during the day, the model air temperature either remains nearly constant (41010) or continues to decrease (41009), missing the diurnal cycle seen in the buoy observations. The Eta Model forcing indicates cold advection along the eastern boundary of the model domain (not shown), which can be implied from the negative air–sea temperature difference at NDBC buoy 41010. This discrepancy suggests that the model sensible heat

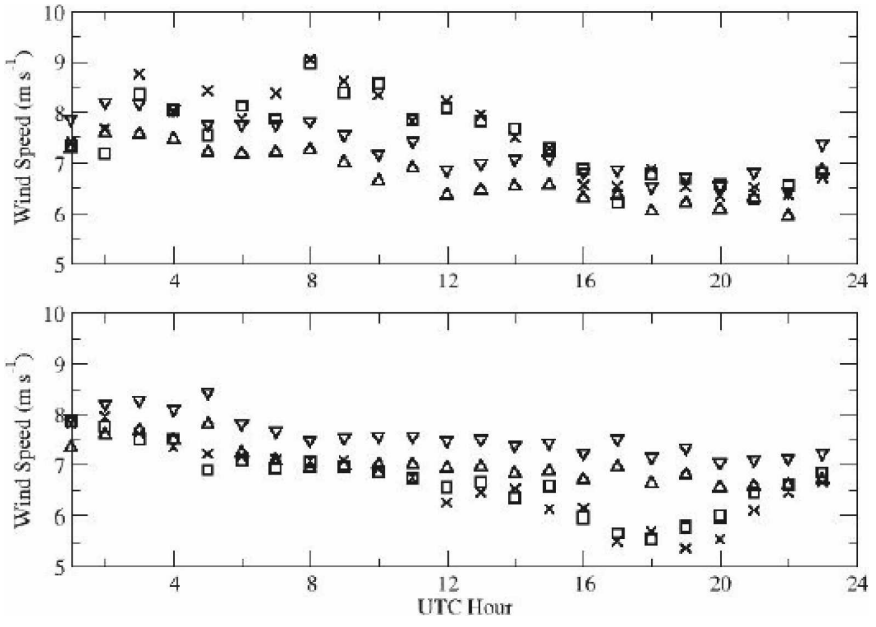

FIG. 21. Hourly averaged wind speeds ($m\ s^{-1}$) for the easterly-flow regime at NDBC buoys (top) 41009 and (bottom) 41010. Buoy (upward-pointed triangle), buoy adjusted to 10 m (downward-pointed triangle), MODIS (square), and RTG (times sign) are shown.

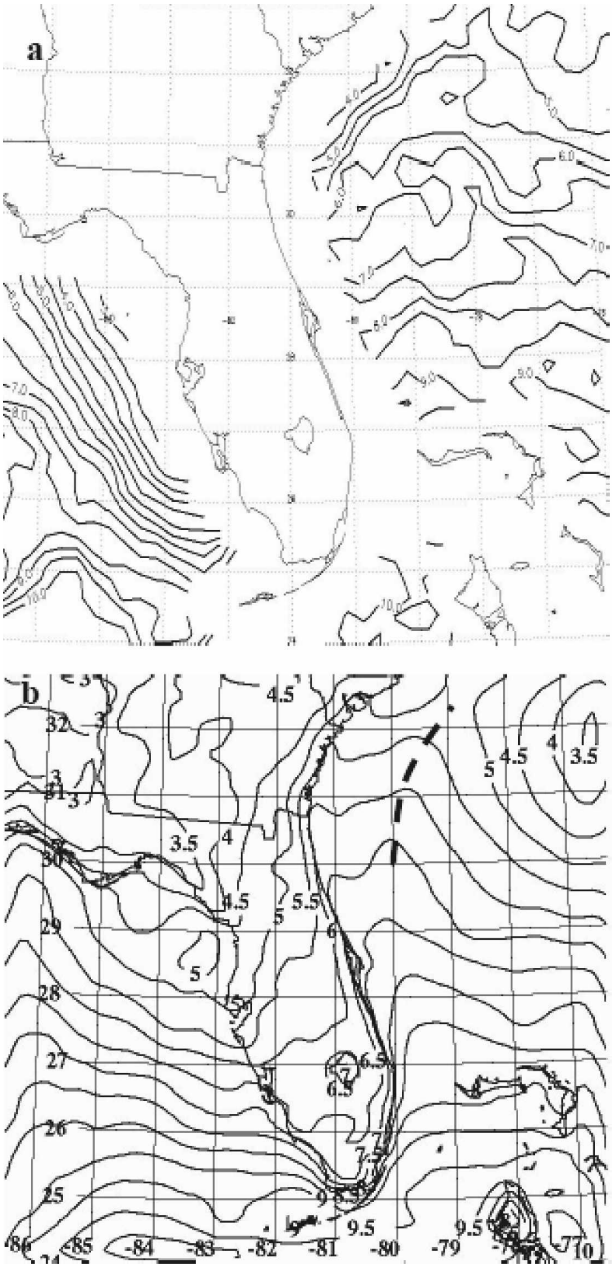

FIG. 22. (a) TMI wind speed average (m s^{-1}) for the period of 10–19 May 2004. (Data courtesy of Remote Sensing Systems, Santa Rosa, CA.) (b) WRF MODIS run average wind speed for the easterly-flow-regime cases: 9, 11–19 May 2004. The hatched line represents a relative maximum in wind speed not observed in the TMI data.

flux may be to low for both the MODIS and RTG simulations.

5. Summary and conclusions

In this study, parallel simulations were studied to determine the impact of high-resolution SSTs on short-term forecasts in the Florida region. The simulations used either the RTG SST analysis or the 1-km MODIS SST composite as a lower boundary condition for a 24-h WRF forecast. RUC analyses, surface, and upper-air observations were assimilated using ADAS, providing the initial conditions for the WRF. Two simulations were performed for each day during May 2004. Results focused on the impact of the simulations within the MABL. A unique aspect of this study, which is in contrast to previous work (e.g., Song et al. 2006), is the realistic nature of the modeled SST. The modifications to the SST here are complex as opposed to idealized adjustments (step function changes, gradient versus no gradient, etc.).

The impact of the high-resolution MODIS SST composite was observable through a comparison of individual simulations, including earlier onset and more vigorous HCRs, elongated/more intense zones of convergence, and an increase in precipitation. Aggregates of model output were used to evaluate the impact of high-resolution SSTs in easterly and westerly dominated low-level flow. Surface heat flux changes associated with the use of the MODIS SST product were directly correlated to SST changes between the SST products. Upward sensible heat fluxes over the Florida Current were larger with the MODIS SST product, while enhanced downward sensible heat fluxes occurred over the cooler waters of the Florida–Hatteras shelf. Vertical wind stress divergence and pressure gradient accelerations across the Florida Current region vary in importance as a function of flow direction and stability. The most significant increase in surface winds in the MODIS simulations occurred during the stable westerly flow regime, with vertical wind stress divergence being the dominant factor. In particular, our results along SST gradient regions in easterly flow simulations are influenced by the significant heat content added upwind. The relative importance of the pressure gradient forcing throughout the MABL in this study is influenced by this effect. The warmer Florida Current present in the MODIS product results in enhanced vertical heat transport that is advected downwind, modifying the thermal structure (e.g., boundary layer depth) and the MABL wind field primarily through pressure gradient adjustments. The adjustments are carried up and over the cooler shelf waters in the easterly flow simulations. The deeper mixed layer in the easterly flow cases yields a response to the surface forcing that is more extensive in the vertical. Validation of the WRF runs with buoy and TMI data indicated that the use of the higher-resolution SST product led to small improvements.

Future work can be extended to investigate the impact of the MODIS SST composites on the daytime

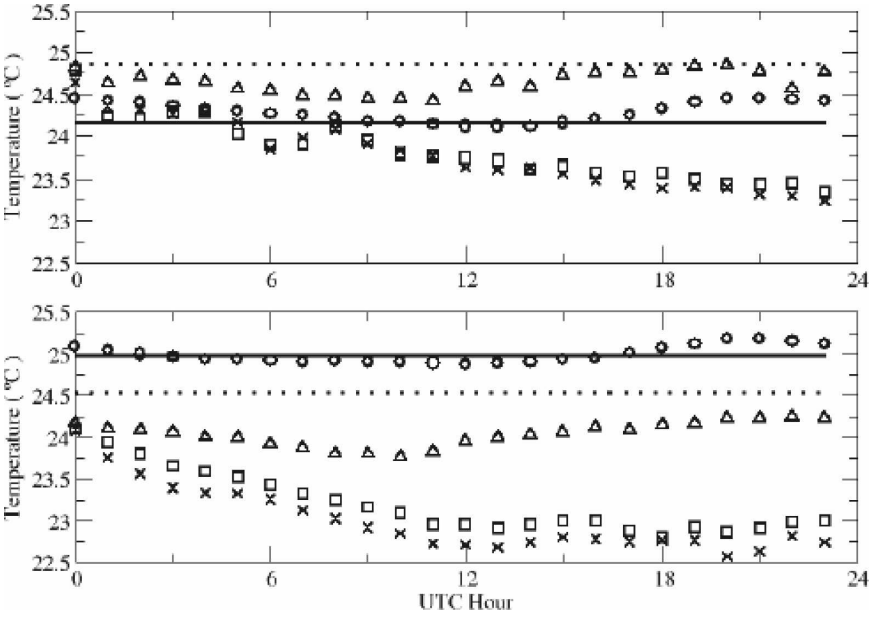

FIG. 23. Hourly averaged surface air and sea surface temperatures (°C) for the easterly-flow regime at NDBC buoys (top) 41009 and (bottom) 41010. Buoy air temperature (upward-pointed triangles), buoy SST (circles), MODIS air temperature (squares), RTG air temperature (times signs), MODIS SST (solid line), and RTG SST (dashed line) are shown.

forecast and to examine days when the mean flow is parallel to the SST gradient. Relevant studies that address the impact of SST resolution during other seasons, in particular the wet season, would also be of benefit. Additionally, updating the SSTs within the forecast cycle would help to evaluate the relative importance of the SST diurnal cycle. As one reviewer pointed out, the frequent availability of analyzed high-resolution SSTs (e.g., Lazarus et al. 2007) might decrease the need to couple mesoscale atmospheric models with ocean models for short-term forecasts.

Acknowledgments. The authors thank Gary Jedlovec and Stephanie Haines for their assistance with the MODIS SST composites. We also thank Jonathan Case, Shih-Hung Chou, and Dennis Buechler for their useful comments with this manuscript. In addition we thank two anonymous reviewers for their helpful comments. This research was funded by the NASA Science Mission Directorate in support of the Short-term Prediction Research and Transition (SPoRT) program at Marshall Space Flight Center.

REFERENCES

Angevine, W. M., M. Tjernström, and M. Žagar, 2006: Modeling of the coastal boundary layer and pollutant transport in New England. *J. Appl. Meteor. Climatol.,* **45,** 137–154.

Bauman, W. H., III, and S. Businger, 1996: Nowcasting for space shuttle landings at Kennedy Space Center, Florida. *Bull. Amer. Meteor. Soc.,* **77,** 2295–2305.

Bratseth, A. M., 1986: Statistical interpolation by means of successive corrections. *Tellus,* **38A,** 439–447.

Brewster, K., 1996: Application of a Bratseth analysis scheme including Doppler radar data. Preprints, *15th Conf. on Weather Analysis and Forecasting,* Norfolk, VA, Amer. Meteor. Soc., 92–95.

Chelton, D. B., 2005: The impact of SST specification on ECMWF surface wind stress fields in the eastern tropical Pacific. *J. Climate,* **18,** 530–550.

——, and Coauthors, 2001: Observations of coupling between surface wind stress and sea surface temperature in the eastern tropical Pacific. *J. Climate,* **14,** 1479–1498.

Chen, F., and J. Dudhia, 2001: Coupling an advanced land surface–hydrology model with the Penn State–NCAR MM5 modeling system. Part I: Model implementation and sensitivity. *Mon. Wea. Rev.,* **129,** 569–585.

Dawson, D. T., II, and M. Xue, 2006: Numerical forecasts of the 15–16 June 2002 southern plains mesoscale convective system: Impact of mesoscale data and cloud analysis. *Mon. Wea. Rev.,* **134,** 1607–1629.

Haines, S. L., G. J. Jedlovec, and S. M. Lazarus, 2007: A MODIS sea surface temperature composite for regional applications. *IEEE Trans. Geosci. Remote Sens.,* **45,** 2919–2927.

Hashizume, H., S.-P. Xie, M. Fujiwara, M. Shiotani, T. Watanabe, Y. Tanimoto, W. T. Liu, and K. Takeuchi, 2002: Direct observations of atmospheric boundary layer response to SST variations associated with tropical instability waves over the eastern equatorial Pacific. *J. Climate,* **15,** 3379–3393.

Hong, S.-Y., Y. Noh, and J. Dudhia, 2006: A new vertical diffusion package with an explicit treatment of entrainment processes. *Mon. Wea. Rev.,* **134,** 2318–2341.

Hsu, S. A., E. A. Meindl, and D. B. Gilhousen, 1994: Determining the power-law wind-profile exponent under near-neutral stability conditions at sea. *J. Appl. Meteor.,* **33,** 757–765.

Janjić, Z. I., 1994: The step-mountain Eta coordinate model: Further developments of the convection, viscous sublayer, and turbulence closure schemes. *Mon. Wea. Rev.,* **122,** 927–945.

Koračin, D., and D. P. Rogers, 1990: Numerical simulations of the response of the marine atmosphere to ocean forcing. *J. Atmos. Sci.,* **47,** 592–611.

Lazarus, S. M., C. M. Ciliberti, J. D. Horel, and K. A. Brewster, 2002: Near-real-time applications of a mesoscale analysis system to complex terrain. *Wea. Forecasting,* **17,** 971–1000.

——, C. G. Calvert, M. E. Splitt, P. Santos, D. W. Sharp, P. F. Blottman, and S. M. Spratt, 2007: Real-time, high-resolution, space–time analysis of sea surface temperatures from multiple platforms. *Mon. Wea. Rev.,* **135,** 3158–3173.

Lericos, T. P., H. E. Fuelberg, A. I. Watson, and R. L. Holle, 2002: Warm season lightning distributions over the Florida peninsula as related to synoptic patterns. *Wea. Forecasting,* **17,** 83–98.

Li, X., W. Zheng, W. G. Pichel, C.-Z. Zou, P. Clemente-Colón, and K. S. Friedman, 2004: A cloud line over the Gulf Stream. *Geophys. Res. Lett.,* **31,** L14108, doi:10.1029/2004GL019892.

Lindzen, R. S., and S. Nigam, 1987: On the role of sea surface temperature gradients in forcing low-level winds and convergence in the Tropics. *J. Atmos. Sci.,* **44,** 2418–2436.

Lorenc, A. C., 1995: Atmospheric data assimilation. Met Office, Scientific Paper 34, 17 pp.

Maloney, E. D., and D. B. Chelton, 2006: An assessment of the sea surface temperature influence on surface wind stress in numerical weather prediction and climate models. *J. Climate,* **19,** 2743–2762.

Mellor, G. L., and T. Yamada, 1982: Development of a turbulence closure model for geophysical fluid problems. *Rev. Geophys. Space Phys.,* **20,** 851–875.

Minnett, P. J., 2003: Radiometric measurements of the sea-surface skin temperature: The competing roles of the diurnal thermocline and the cool skin. *Int. J. Remote Sens.,* **24,** 5033–5047.

——, R. H. Evans, O. Brown, E. Key, G. Szczodrak, K. Kilpatrick, W. Baringer, and S. Walsh, cited 2007: MODIS sea-surface temperatures for GHRSST-PP. Preprints, *GHRSST-PP Sixth Science Team Meeting,* Exeter, United Kingdom, Met Office. [Available online at http://ghrsst-pp.metoffice.com/pages/meetings/workshop6/Presentations/19th/Minnett-Evans-RSMAS_GHRSST6_200519-release.ppt.]

NCDC, cited 2004: Climate of 2004—May Florida drought. [Available online at http://www.ncdc.noaa.gov/oa/climate/research/2004/may/st008dv00pcp200405.html.]

Nonaka, M., and S.-P. Xie, 2003: Covariations of sea surface temperature and wind over the Kuroshio and its extension: Evidence for ocean-to-atmosphere feedback. *J. Climate,* **16,** 1404–1413.

O'Neill, L. W., D. B. Chelton, and S. K. Esbensen, 2003: Observations of SST-induced perturbations of the wind stress field over the Southern Ocean on seasonal timescales. *J. Climate,* **16,** 2340–2354.

——, ——, ——, and F. J. Wentz, 2005: High-resolution satellite measurements of the atmospheric boundary layer response to SST variations along the Agulhas Return Current. *J. Climate,* **18,** 2706–2723.

Raman, S., N. C. Reddy, and D. S. Niyogi, 1998: Mesoscale analysis of a Carolina coastal front. *Bound.-Layer Meteor.,* **86,** 125–145.

Rouault, M., A. M. Lee-Thorp, and J. R. E. Lutjeharms, 2000: The atmospheric boundary layer above the Agulhas Current during alongcurrent winds. *J. Phys. Oceanogr.,* **30,** 40–50.

——, C. J. C. Reason, J. R. E. Lutjeharms, and A. C. M. Beljaars, 2003: Underestimation of latent and sensible heat fluxes above the Agulhas Current in NCEP and ECMWF analyses. *J. Climate,* **16,** 776–782.

Samelson, R. M., E. D. Skyllingstad, D. B. Chelton, S. K. Esbensen, L. W. O'Neill, and N. Thum, 2006: On the coupling of wind stress and sea surface temperature. *J. Climate,* **19,** 1557–1566.

Skamarock, W. C., J. B. Klemp, J. Dudhia, D. O. Gill, D. M. Barker, W. Wang, and J. G. Powers, 2005: A description of the advanced research WRF version 2. NCAR Tech. Note NCAR/TN-468+ STR, 88 pp.

Skyllingstad, E. D., R. M. Samelson, L. Mahrt, and P. Barbour, 2005: A numerical modeling study of warm offshore flow over cool water. *Mon. Wea. Rev.,* **133,** 345–361.

Small, R. J., S.-P. Xie, and Y. Wang, 2003: Numerical simulation of atmospheric response to Pacific tropical instability waves. *J. Climate,* **16,** 3723–3741.

Song, Q., T. Hara, P. Cornillon, and C. A. Friehe, 2004: A comparison between observations and MM5 simulations of the marine atmospheric boundary layer across a temperature front. *J. Atmos. Oceanic Technol.,* **21,** 170–178.

——, P. Cornillon, and T. Hara, 2006: Surface wind response to oceanic fronts. *J. Geophys. Res.,* **111,** C12006, doi:10.1029/2006JC003680.

Sublette, M. S., and G. S. Young, 1996: Warm-season effects of the Gulf Stream on mesoscale characteristics of the atmospheric boundary layer. *Mon. Wea. Rev.,* **124,** 653–667.

Thiébaux, J., E. Rogers, W. Wang, and B. Katz, 2003: A new high-resolution blended real-time global sea surface temperature analysis. *Bull. Amer. Meteor. Soc.,* **84,** 645–656.

Tijm, A. B. C., A. A. M. Holtslag, and A. J. van Delden, 1999: Observations and modeling of the sea breeze with the return current. *Mon. Wea. Rev.,* **127,** 625–640.

Tokinaga, H., Y. Tanimoto, and S.-P. Xie, 2005: SST-induced surface wind variations over the Brazil–Malvinas confluence: Satellite and in situ observations. *J. Climate,* **18,** 3470–3482.

——, and Coauthors, 2006: Atmospheric sounding over the winter Kuroshio Extension: Effect of surface stability on atmospheric boundary layer structure. *Geophys. Res. Lett.,* **33,** L04703, doi:10.1029/2005GL025102.

Troen, I. B., and L. Mahrt, 1986: A simple model of the atmospheric boundary layer; sensitivity to surface evaporation. *Bound.-Layer Meteor.,* **37,** 129–148.

Wallace, J. M., T. P. Mitchell, and C. Deser, 1989: The influence of sea-surface temperature on surface wind in the eastern equatorial Pacific: Seasonal and interannual variability. *J. Climate,* **2,** 1492–1499.

Warner, T. T., M. N. Lakhtakia, J. D. Doyle, and R. A. Pearson, 1990: Marine atmospheric boundary layer circulations forced by Gulf Stream sea surface temperature gradients. *Mon. Wea. Rev.,* **118,** 309–323.

Xue, M., and W. J. Martin, 2006: A high-resolution modeling study of the 24 May 2002 dryline case during IHOP. Part I: Numerical simulation and general evolution of the dryline and convection. *Mon. Wea. Rev.,* **134,** 149–171.

——, K. K. Droegemeier, and V. Wong, 2000: The Advanced Regional Prediction Systems (ARPS)—A multi-scale nonhydrostatic atmospheric simulation and prediction model. Part I: Model dynamics and verification. *Meteor. Atmos. Phys.,* **75,** 161–193.

Zhang, F., A. M. Odins, and J. W. Nielsen-Gammon, 2006: Mesoscale predictability of an extreme warm-season precipitation event. *Wea. Forecasting,* **21,** 149–166.